Empowering a coupled hydrological-geotechnical model to simulate long-term vegetation dynamics and their impact on catchment-scale flood and landslide hazards

Chen, Guoding; Zhang, Ke; Li, Yunping; Feng, Jin; Bogaard, Thom

DOI
10.1016/j.jhydrol.2025.133225

Publication date
2025

Document Version
Final published version

Published in
Journal of Hydrology

Citation (APA)
Chen, G., Zhang, K., Li, Y., Feng, J., & Bogaard, T. (2025). Empowering a coupled hydrological-geotechnical model to simulate long-term vegetation dynamics and their impact on catchment-scale flood and landslide hazards. *Journal of Hydrology*, *658*, Article 133225. https://doi.org/10.1016/j.jhydrol.2025.133225

Journal of Hydrology 658 (2025) 133225

Contents lists available at ScienceDirect

Journal of Hydrology

journal homepage: www.elsevier.com/locate/jhydrol

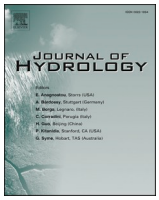

Research papers

Empowering a coupled hydrological-geotechnical model to simulate long-term vegetation dynamics and their impact on catchment-scale flood and landslide hazards

Guoding Chen [a,b], Ke Zhang [a,c,*], Yunping Li [a], Jin Feng [a], Thom Bogaard [b]

[a] National Key Laboratory of Water Disaster Prevention, College of Hydrology and Water Resources, and Yangtze Institute for Conservation and Development, Hohai University, Nanjing, Jiangsu 210098, China
[b] Delft University of Technology, Faculty of Civil Engineering and Geosciences, Department of Water Management, Stevinweg 1, 2628 CN Delft, the Netherlands
[c] China Meteorological Administration Hydro-Meteorology Key Laboratory, Hohai University, Nanjing, Jiangsu, 210024, China

ARTICLE INFO

This manuscript was handled by Sally Elizabeth Thompson, Editor-in-Chief, with the assistance of Shuolin Li, Associate Editor

Keywords:
Vegetation dynamics
Root reinforcement
Hydrological-geotechnical models
3D slope stability model
Flood-landslide events

ABSTRACT

Vegetation plays a critical role in regulating the catchment water balance and enhancing soil stability through root reinforcement. The dynamic nature of vegetation, particularly its seasonal change, significantly affects the magnitude of this influence. However, quantifying the long-term impacts of dynamic vegetation on both flood and landslide occurrences at the catchment scale remains challenging due to the complexity of root structures and the varying dimensions of landslides. In this study, we improved the coupled hydrological-geotechnical model iHydroSlide3D v1.0 by incorporating key vegetation components, such as Leaf Area Index (LAI), root characteristics, and their seasonal dynamics. The improved model was validated using historical observations and applied to a 100-years simulation driven by a weather generator. Three computational scenarios were employed to assess the influence of vegetation on key hydrological and slope-stability variables. Results show that vegetation reduces soil moisture and runoff during low to moderate rainfall events but has a limited impact during larger rainfall events. Additionally, slope stability is found to be more influenced by root reinforcement than soil water uptake. The dynamic nature of vegetation plays a decisive role in modulating its effects on hydrological processes and soil stability, depending on the growth or decay trend of vegetation. This modeling framework offers a robust tool for assessing long-term flood and landslide risks in vegetated catchments.

1. Introduction

Floods and landslides are widespread and severe natural hazards, posing significant threats to lives and property worldwide (Hong et al., 2006; Zhang et al., 2022b; Yanfatriani et al., 2024). Runoff and soil erosion could occur in a cascading manner during a heavy-rainfall period triggering both floods and landslides combined (Lin et al., 2008; Zhang et al., 2016; Al-Omari et al., 2024). The vegetation has an important role in linking the atmospheric and terrestrial systems (Xu et al., 2016; Zhang et al., 2019a; Ma et al., 2022). Vegetation profoundly impacts water budgets (Li et al., 2018; Luo et al., 2020a), soil erosion and hillslope stability (Schwarz et al., 2012; Evette et al., 2009). From a hydrogeotechnical point of view, vegetation has both hydrological and mechanical effects (Coppin and Richards, 1990; Stokes et al., 2014; Bordoloi and Wang Wai Ng, 2020; Gilmour, 1968). The hydrological effect is mainly a reduction of available water via interception evaporation and transpiration via root water uptake from the soil. The reduction of water amount further changes the soil pore-water pressure, which, in turn, affects the soil unsaturated hydraulic conductivity and shear strength (Lu and Godt, 2013; Liu et al., 2016; Feng et al., 2020). The mechanical effect refers to the additional reinforcement provided by roots against driving forces acting on potential landslides (Pollen and Simon, 2005; Schwarz et al., 2010b). Trees exert substantial influence on the initiation of shallow landslides in steep, forested watersheds, particularly during intense storm events (Kim et al., 2013; Schwarz et al., 2013). Examination of landslide scars frequently discloses fractured root tendrils, indicating the activation of root tensile strength during failure (Schmidt et al., 2001). Several field studies have supported the impact of vegetation on reducing peak flow discharge (Green and Alila, 2012; Kuraś et al., 2012; Zhao et al., 2016; Bathurst et al.,

* Corresponding author.
E-mail address: kzhang@hhu.edu.cn (K. Zhang).

https://doi.org/10.1016/j.jhydrol.2025.133225
Received 4 October 2024; Received in revised form 15 January 2025; Accepted 30 March 2025
Available online 3 April 2025

2020). Others have experimentally quantified the influence of vegetation cover on soil erosion and surface runoff in loess areas (Chen et al., 2007; El Kateb et al., 2013; Zhang et al., 2014; Chen et al., 2018). However, both laboratory and field experiments are generally cost-prohibitive, particularly for large-scale and extended studies, rendering them impractical for quantifying the long-term effects of vegetation. Additionally, the results are challenging to extrapolate to other regions. In lieu of this, mathematical models present affordable alternatives for quantifying how and to what extent vegetation could influence hydrological and landslide behaviour, particularly over decadal and longer timescales (Schwarz et al., 2013; Parr et al., 2015; Arnone et al., 2016; Xu et al., 2016; Zhang et al., 2022a).

The construction of model frameworks within the soil–plant-atmosphere continuum has been widely undertaken to quantify the role of vegetation (Katul et al., 2012). When considering root reinforcement in soil stability, a common simplification involves assuming a static root distribution underground, achieved through analytical methods (Ng et al., 2015; Liu et al., 2016; Feng et al., 2020) or utilizing measured root architectures (Wu et al., 1979; Ekanayake and Phillips, 1999; Pollen, 2007), with the approach of Wu et al. (1979) being frequently incorporated. Given the assumption in Wu's model that all roots break simultaneously, the potential for overestimation of increased soil shear strength exists (Waldron and Dakessian, 1981). As an alternative, Fiber Bundle Models (FBM) consider the maximum load for a bundle of fibers to be less than the sum of each individual strength (Pollen and Simon, 2005). FBM demonstrates superior performance in relation to laboratory and field tests compared to the Wu/Waldron model (Wu et al., 1979; Waldron, 1977). Building upon these advances, Schwarz et al. (2010a) introduced the strain-step loading approach in the Root Bundle Model (RBM). The application of RBM facilitates the assessment of shallow landslides by better considerations of root reinforcement (Cislaghi et al., 2017; Cislaghi et al., 2018; Bordoni et al., 2024). Accounting for the vegetative state, there exists a subset of methods that focuses on the dynamic simulation or remote sensing-based LAI, effectively enhancing the performance of hydrological models by refining the simulations of interception evaporation and transpiration (e.g., Parr et al., 2015; Tesemma et al., 2015; Alemayehu et al., 2017; Bai et al., 2018). The effects of root system growth have been investigated through the incorporation of more or less complex growth models, such as L-Systems (Leitner et al., 2010) and RootBox (De Moraes et al., 2018). These functional representations have also been integrated into the HYDRUS software packages, accommodating various environmental factors and soil hydraulic properties (Hartmann et al., 2018).

Combined flood-landslide events are infrequently analyzed collectively, with the important role of vegetation is often overlooked. Furthermore, at catchment or larger scales, predominantly, infinite (1D) slope stability models have been employed to assess stability under vegetation cover due to their ease of implementation and interpretation (Ng et al., 2015; Arnone et al., 2016). A limitation associated with 1D models is the challenge in incorporating the intricate architecture of the root system, leading to a failure to consider the contribution of lateral reinforcement (Schwarz et al., 2010a; Cislaghi et al., 2017). Recent work using three-dimensional (3D) slope stability models have effectively addressed the inclusion of root systems within the soil (Cislaghi et al., 2017; Schmaltz and Mergili, 2018). This advancement significantly enhances the scope of simulation scenarios. However, landslide events are frequently perceived as isolated occurrences, with limited consideration given to changes in hydrological variables, including vegetation dynamics. The intricate impact of vegetation in catchment-scale flood-landslide cascading events has rarely been quantified. Additionally, in the context of long-term modeling, it is imperative to reasonably depict the dynamics of vegetation (i.e., growth and decay) (Parr et al., 2015; Zhang et al., 2022a; Rattanarat et al., 2024). To date, achieving a fully coupled simulation and analysis with time-dependent vegetation characteristics to assess flood generation and slope stability (3D) jointly remains elusive. To the best of our knowledge, this study presents the first such modeling endeavour.

In this work, we improved the open-source modeling framework iHydroSlide3D v1.0 (Chen et al., 2023) by integrating dynamic vegetation components as a submodule. Following parameterization and validation processes, the model was utilized to perform long-term simulations driven by climatic variables generated through a weather generator. By defining various simulation scenarios, we investigated the impact of vegetation on both flood generation and landslide initiation, examining aspects of soil water dynamics, root reinforcement, and vegetation dynamics. This paper is organized as follows. Section 2 describes the key enhancements made to iHydroSlide3D v1.0, the methodology for long-term hazards assessment, and the method for parameter sensitivity analysis. Section 3 introduces the study area, model inputs, simplifications, and the computational scenarios employed. Section 4 details the model results of vegetation and its effect on flood-landslide events. Then we discuss the obtained results in Section 5, and the conclusions are described in Section 6.

2. Methods

2.1. iHydroSlide3D v1.0 model

A coupled hydrological-geotechnical model, iHydroSlide3D v1.0 (Chen et al., 2023), served as the foundational framework for the study. iHydroSlide3D v1.0 is an open-source model rooted in physical principles, operating through the integration of a distributed hydrological model (CREST) (Wang et al., 2011) and a three-dimensional (3D) slope stability model. The model ensures a complete balance of water between the surface and subsurface systems and traces the development of pore-water pressure and water table for slope instability. iHydroSlide3D v1.0 follows the modeling concept of r.slope.stability (Mergili et al., 2014), which involves the random generation of a significant number of ellipsoidal slip surfaces across a specified region. The values of the landslide size (length, width, and depth), and the location of the centre are generated separately for each ellipsoid using a simple pseudo-random algorithm based on the user-defined restriction (maximum and minimum values in Table S1). Each potential landslide is discretized into multiple soil columns, each associated with varying states of soil water and strength (Chen et al., 2023). Consequently, several ellipsoids may intersect the same sliding surface (and vice versa), necessitating a convergence calculation to achieve reliable landslide susceptibility mapping at a catchment scale. The model is underpinned by a modular framework, providing the option to employ different simulation resolutions within submodules, facilitated by a method of soil moisture downscaling (Wang et al., 2020). The iHydroSlide3D v1.0 has the capacity to generate outputs for the factor of safety (F_s), probability of landslide occurrence (P_f), as well as details regarding landslide area (A_L) and landslide volume (V_L). Further detailed information can be found in the work of Chen et al. (2023).

2.2. Integration of vegetation components in iHydroSlide3D v1.0

2.2.1. Evapotranspiration (ET)

The initial CREST model family relies on meteorological data, specifically rain and evapotranspiration (ET) series, and does not actively calculate ET values (Li et al., 2021; Chen et al., 2023; Flamig et al., 2020). This fashion proves effective in scenarios where measured or satellite-derived data is accessible; however, it encounters challenges in establishing connections with vegetation dynamics. In this work, MODIS ET algorithm (Mu et al., 2011) was used to estimate ET based on the logic of the Penman-Monteith equation. It leverages the surface energy balance principle, considering parameters such as land surface temperature, vegetation properties, and meteorological data. The Leaf Area Index (LAI) value serves as a key parameter in the algorithm, and its dynamic simulation method is elucidated in Section 2.2.3.

2.2.2. Root reinforcement and slope stability

Roots enhance soil stability through three mechanisms: basal root reinforcement, lateral root reinforcement, and stiffening effects under compression (Vergani et al., 2017). The basal reinforcement is the most efficient when roots intersect the slip surfaces of a shallow landslide, reaching the underlying strata (e.g., Fig. 1b). In instances where roots fail to penetrate the failure surface (Fig. 1c), their stabilizing effect is reduced. In such cases, the primary role of the roots is to enhance soil stability through lateral reinforcement (Schwarz et al., 2010b). In this work, we incorporated a branching topology model (Arnone et al., 2016) into iHydroSlide3D v1.0 to estimate the root reinforcement. This model is founded on Leonardo's rule, which posits a correlation between adjacent branches, taking into account the root diameter and the root count at two consecutive levels (Arnone et al., 2016; Preti et al., 2022) (see Fig. 1a):

$$d_j = d_{j-1}\sqrt{\frac{1}{\alpha_d}\frac{N_{j-1}}{N_j}}, \tag{1}$$

where α_d is a proportionality factor that can be fitted based on the observed root area at various depths; d_j and N_j is the diameter and number of branches at the topological level j, respectively. We initially adopted the premise that the number of root at the generic topological level could be estimated by a specific probability density function (Arnone et al., 2016). However, we modified the formula by introducing a constant value within a very shallow soil mantle where the root system is naturally characterized by the coexistence of diverse vegetation species. In this study, we employed a piecewise function, selecting a geometric distribution to discretely model the occurrence of root numbers with respect to root depth. For a total number of roots denoted as N_{tot}, the calculation of the number of roots at each topological level (N_j) can be expressed as follows:

$$N(j|p) = \begin{cases} N_c, r \le r_s \\ (N_{tot} - N_c)(1-p)^{k-1}p, r_s < r \le r_{max} \end{cases}, \tag{2}$$

where N_c represents the constant value denoting the root number within the topsoil depth, r_s; p is the parameter of the distribution; r is depth of the root level in soil, extending up to its maximum value r_{max}.

The Root Bundle Model-Weibull (RBMw) (Schwarz et al., 2013; Arnone et al., 2016) is further used to quantify the mechanical reinforcement provided by roots. RBMw is grounded in the foundational concept that a bundle of root fibers cannot all fail simultaneously but rather undergoes a progressive rupture process (Pollen and Simon, 2005). This paradigm shift marks an enhancement contrasted with conventional methods such as the Wu/Waldron model (Wu et al., 1979), which solely aggregates the tensile strength of individual root fibers and, consequently, may lead to potential overestimations (Pollen and Simon, 2005; Pollen, 2007). The tensile force exerted by the bundle of roots, $F_{tot}(\Delta x)$, is derived through summation of the contributions from all roots scaled by the relative probability $S_{d_i}(\Delta x^*)$:

$$F_{tot}(\Delta x) = \sum_{i=1}^{N_{tot}} F_{d_i}(\Delta x) S_{d_i}(\Delta x^*), \tag{3}$$

where i is the generic root fiber and d_i is the root diameter (see in Fig. 1a); Δx and $F_{d_i}(\Delta x)$ collectively establish the force–deformation relationship based on Young's modulus; $S_{d_i}(\Delta x^*)$ is survival probability described by Weibull survival function (Schwarz et al., 2013):

$$S_{d_i}(\Delta x^*) = exp\left[-\left(\frac{\Delta x^*}{\lambda^*}\right)^{\omega}\right], \tag{4}$$

where Δx^* is the normalized displacement, $\Delta x^* = \Delta x/\Delta x_{max,d_i}$; ω is the shape factor of the Weibull function and λ^* is commonly fixed to 1 (Arnone et al., 2016) representing the scaling factor.

The calculated root strength is used to add root-induced cohesion (c_r) into the cohesion term within the framework of iHydroSlide3D v1.0, where the 3D limit equilibrium equation is employed. In the context of potential landslides, c_r is calculated at each soil column element based on the penetration condition of the vegetation root into the slip surface (Fig. 1b and c). This implies that the basal and lateral reinforcement are not considered separately (e.g., as done by Schwarz et al. (2010b)), but are equally computed by precisely accounting for the topological level of the root system.

2.2.3. Vegetation dynamics

The dynamic characteristics of surface vegetation were represented by Leaf Area Index (LAI), which serves as a valuable measure of seasonal canopy dynamics. This study adopted a simple prognostic phenology model, grounded in the influence of environmental factors, to predict the seasonal course of LAI. This model considers three fundamental mechanisms that serve as reliable proxies for leaf lifespan: daily minimum air temperature (T_a), vapor pressure deficit (V_p), and photoperiod (P_h) (Jolly et al., 2005; Stöckli et al., 2008). These variables play a pivotal role in the formulation of the Growing Season Index (G_i) (Jolly et al., 2005):

$$G_i = f_1(T_a) \times f_2(P_h) \times f_3(V_p), \tag{5}$$

where f_1, f_2, and f_3 are transformation functions based on the threshold parameters of above environmental factors, they delineate the manner in which G_i varies within the range of 0 to 1 (Stöckli et al., 2008; Jolly et al., 2005). Subsequently, the dynamic LAI was further simulated as a piecewise linear function of G_i and a threshold parameters (τ) (Savoy and Mackay, 2015):

$$LAI = \begin{cases} LAI_{\min}, & G_i < \tau \\ G_i \times LAI_{\max}, & G_i \ge \tau \end{cases}, \tag{6}$$

where $LAI_{\min}$ and $LAI_{\max}$ are the observed minimum and maximum values. Note that the daily G_i is computed as a moving 21-day mean to prevent canopy changes from being prematurely triggered by single extreme events (Jolly et al., 2005).

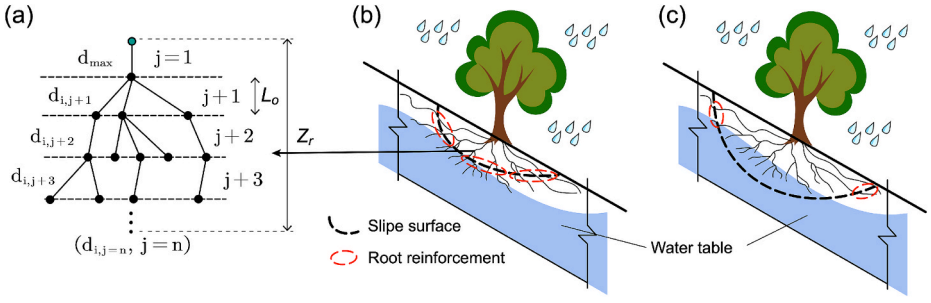

Fig. 1. Conceptualization of (a) the root topological model and a representative ellipsoid used as the slip surface. Root strength is exerted in the form of (b) basal reinforcement and (c) lateral reinforcement, depending on dimensions of the potential shallow landslide.

The dynamics of subsurface vegetation pertain to the variations in root biomass (B_{root}), which are closely associated with root profiles and play a crucial role in soil mechanical behavior (Alam et al., 2021). Due to the typically limited availability of root system data in most cases, estimations are commonly carried out using either empirical methods (Addo-Danso et al., 2016) or physical modeling (Hartmann et al., 2018; Leitner et al., 2010; Tron et al., 2015). An essential connection between remote sensing and root traits involves the utilization of a regressive relationship that begins with Leaf Area Index (LAI) and subsequently translates it into aboveground biomass (Nwobi and Williams, 2021):

$$\log B_g = c_1 + c_2 \bullet LAI. \tag{7}$$

Following closely behind, an allometric relationship between B_{root} and shoot biomass (B_g) is recommended as (Coyle et al., 2008):

$$\ln B_{root} = c_3 \cdot ln B_g + c_4 .\# \tag{8}$$

The parameters c_1, c_2, c_3, and c_4 are regression fitting coefficients. This approach simplifies the intricate composition of biomass and yields a preliminary estimate, and the vegetation classification at a stand-scale is not required (Sloan et al., 2013). The resulting B_{root} is reflected in root diameters, assuming that material density and N_{tot} remain unaffected, and subsequently, it is returned to the calculation of root strength (Eq. (3)). The proportion of changing biomass is equitably distributed among all roots in a quadratic relationship. These regression models indicate that LAI and B_{root} share a common trait in terms of vegetation growth and decay. This phenomenon has been observed consistently across regions exhibiting distinct seasonal climate variations, reinforcing the feedback loop with root biomass dynamics (Du et al., 2019; Meinen et al., 2009). Similar regression relationships have also found application in vegetated areas for fitting observed root data (Lai et al., 2013) and assessing forest dynamics in situations where root data are lacking (Sloan et al., 2013).

2.3. Assessing hazards in long-term modeling

We selected the annual maximum peak flow (Q_{max}) at the catchment outlet and regional landslide hazard index (R_L) to evaluate floods and landslides. The adoption of a simple annual landslide initiation index may yield inconclusive results when comparing different years, primarily due to the strong correlation between instability calculations and soil wetness, which exhibits noticeable seasonality. The R_L employed in this study represents a more dynamic and comprehensive index, taking into account both the landslide probability (P_f) and landslide volume (V_L). The definition of R_L originates from specific values of P_f and V_L at a generic pixel, with an integral defined as the product of them over a specified time period:

$$R_{pixel} = \int P_f \times V_L \, dt. \tag{9}$$

Summarizing the R_{pixel} over the region yields the regional landslide hazard, R_L. The integral interval is defined as the wet months with accumulated rainfall (P_{acc}) exceeding accumulated evapotranspiration (ET_{acc}) (Setiawan, 2020) (Fig. 2). We excluded dry seasons from the integral interval to enhance the precision of capturing rainfall events. Considering the shifting length of wet and dry seasons allow us to analyse the hydrological and ecological dynamics in the timing of water availability. Using R_L helps identify cases in which a larger landslide threat could exist during a period when there is a relatively low probability but a significant magnitude (e.g., t_3 to t_4 in Fig. 2). The combination of R_L and Q_{max} is further utilized to determine the exceedance probability (i.e., frequency distribution) by ranking their magnitude in descending order (Green and Alila, 2012).

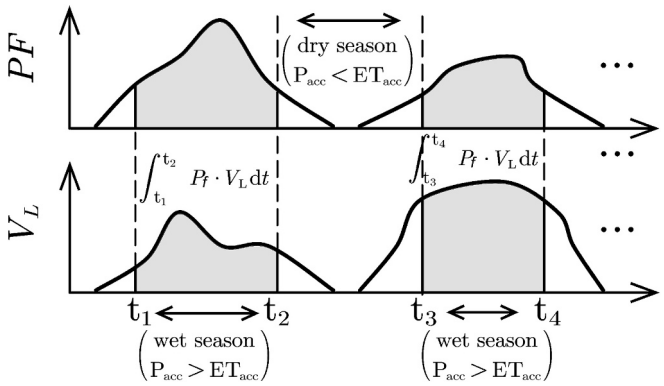

Fig. 2. Assessing method for landslide hazards in a long-term period, where the landslide probability, magnitude, and lasting time are considered.

2.4. Parameter sensitivity analysis

In addition to the essential parameters included in the original iHydroSlide3D v1.0, this study introduces additional parameters related to vegetation (Table S1). The modeling parameters are classified into two categories: hydrological parameters and regional 3D slope stability parameters. To evaluate the sensitivity of the model parameters, a one-factor-at-a-time (OAT) approach was employed, wherein each parameter was varied independently while keeping all other parameters constant. The outcomes of the OAT analysis were assessed using a sensitivity index (S_I), which was calculated based on central differences for the derivatives (Lenhart et al., 2002; Luo et al., 2008):

$$S_I = \frac{\Delta P}{\Delta I}\frac{I}{P(I)} = \frac{P(I+\Delta I) - P(I-\Delta I)}{2\Delta I}\frac{I}{P(I)}. \tag{10}$$

Here, P represents the dependent variable in the sensitivity analysis, while I is the input parameter. The absolute value of S_I quantifies the degree of sensitivity of the target parameters to model predictions, with a larger absolute value corresponding to a higher sensitivity. For parameters calibrated within specific ranges (see Table S1), their values were incremented by 10 % across the defined interval. For parameters determined by the input datasets or users, their values were varied by ±10 % of the assigned values provided in Table S1. In this study, the total runoff volume at the outlet and the regional unstable area were selected as the target variables of interest.

3. Case study and model scenarios

3.1. Study area

The case study area is the upstream part of the Yuehe River Basin located in Shaanxi Province, China. This area covers a total area of 257 km^2 and the elevation ranges from 200 to 1800 m (Fig. 3a). The climate shows strong seasonality with most of the precipitation falling from June to October with an average annual value of 984 mm/yr. The average daily temperature ranges from −1 °C to 34 °C, and the average annual ET is 653 mm/yr. No permanent snow or ice is observed. This region is mainly covered by loam soil and the MODIS Land Cover (Sulla-Menashe and Friedl, 2018) shows that the basin is dominated by deciduous broadleaf forests and mixed forests (Fig. 3b). No detailed investigation for tree species is available and the normalized tree biomass dataset (Luo et al., 2020b) roughly shows that the dominant tree species in this area are Pinus tabuliformis and Pinus armandii. The study area is recurrently affected by floods and landslides throughout the annual wet season. A comprehensive examination of historical disasters conducted by the local Geological Survey Office (Wang et al., 2020) documented a total of 39 landslides occurring from 2010 to 2012 (Fig. 3a). Moreover,

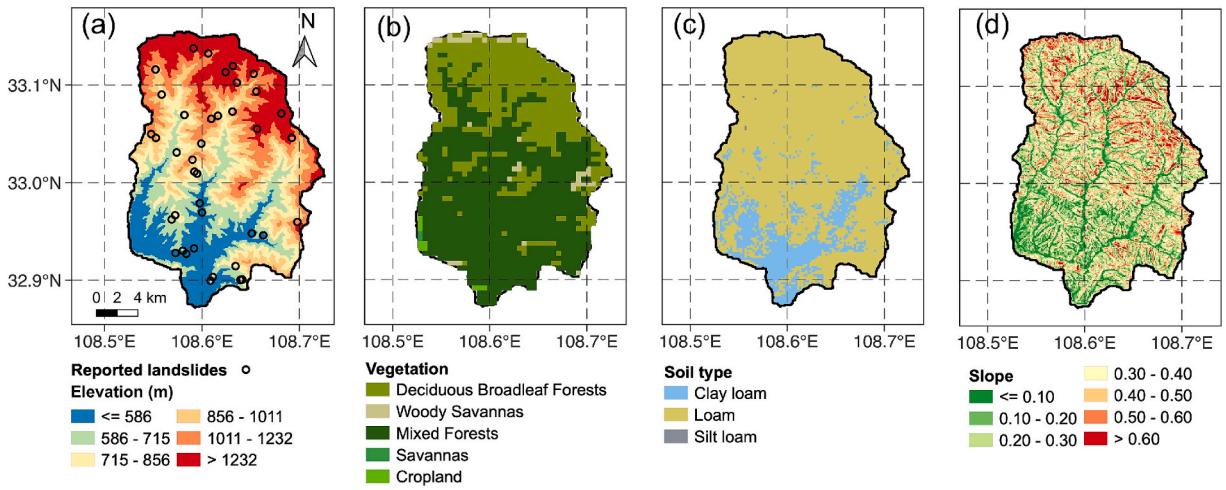

Fig. 3. Study area that chosen as a typical vegetated catchment: (a) elevation and the recorded landslide events; (b) vegetation map; (c) soil type; (d) terrain slope.

rainstorms have been identified as the primary cause of floods, leading to flood-landslide cascading events. The extensively documented information concerning landslide locations and hydrographs, encompassing both specific disaster events and the long-term timeframe, is subsequently employed for the parameterization and validation of the model. Further elaboration on this matter can be found in Supporting Information S1.

3.2. Materials and parameters

Table 1 summarizes the model inputs. Drawing upon the foundational data stipulated in iHydroSlide3D v1.0 (Chen et al., 2023), this study necessitates additional inputs concerning vegetation components and meteorological forcing for a comprehensive, long-term simulation. Topographic properties and soil texture maps, integral to our study area located within a subbasin of the region where iHydroSlide3D v1.0 was meticulously applied, can be directly extracted from the well-prepared datasets provided by Guoding Chen et al. (2023). The datasets shared among the hydrological and landslide modules have been processed into two resolutions, specifically 90 m and 12 m, respectively. This resolution differentiation facilitates an across-scale simulation between submodules via a soil moisture downscaling method (Chen et al., 2023; Wang et al., 2020).

The rainfall series and other essential climatic variables necessary for the model were generated utilizing AWE-GEN (Fatichi et al., 2011), a numerical tool proficient in replicating numerous statistical properties inherent in meteorological variables. These variables encompass precipitation, cloudiness, shortwave radiation, air temperature, vapor pressure, wind speed, and atmospheric pressure, spanning from hourly intervals to several years. A comprehensive dataset comprising one hundred years (2023–2122) of hourly climatic time series was generated, aligning with the statistical properties derived from meteorological data obtained from a designated meteorological station. The utilization of AWE-GEN necessitates observed climate data covering the period from January 2011 to December 2021, sourced from the Hanyin meteorological station (32°54′N, 108°30′E, 413 m a.s.l.). Evapotranspiration calculations were conducted using the MODIS ET algorithm, which mandates daily-scale input parameters such as LAI and weather data. Calibration of the prognostic phenology model (as detailed in Section 2.2.3) was achieved through the integration of MODIS LAI observations, characterized by a spatial resolution of 500 m and an 8-day interval, spanning the years 2011 to 2021. MODIS cells in the area exhibit a relatively uniform cover of Pinus tabuliformis and Pinus armandii. Subsequently, the calibrated phenology model is applied for LAI prediction throughout the simulation period.

Table 1
Overview of input datasets/maps.

Datasets type	Specific inputs
Topographic properties	Digital elevation model, flow direction, flow accumulation, topographic wetness index, river network, and topographic curvature
Soil texture	The Harmonized World Soil Database (HWSD v1.2) (Wieder et al., 2014)
Inputs for AWE-GEN	Hourly climatic data observed in Hanyin meteorological station from 2011 to 2021
Meteorological forcing for long-term simulation	Climatic variables from 2023 to 2122 generated by AWE-GEN, with a timescale ranging from hourly to several years
Historical LAI	MODIS LAI observations from 2011 to 2021
Root architecture	Root depth, number, diameter, and area
Simulating parameters	Dataset-derived and calibrated values (listed in Table S1)
Calibration/verification data	Investigation of floods and landslides within the study area

The root architectures were parameterized according to values derived from the existing literature and were subsequently employed as the initial conditions for the root system state. The root data was taken from (Cohen et al., 2011; Schwarz et al., 2013; Tron et al., 2014) that was also used by Arnone et al. (2016) to describe the root system for the typical tree and shrub. We adopted them in our tree-dominated area (Fig. 3b). The root depth reaches 1.5 m and the root number for each root level were fixed in this study. The vegetation dynamics for root biomass only leads to the variation of the root diameter, which subsequently affects the root strength. The regressive parameters (see in Table S1) were fitted by available data measuring for loblolly pine (Coyle et al., 2008; Nwobi and Williams, 2021). We inherited the parameters for approximation because (i) the three specie in their region and ours belong to the same specie pooled, Pinus Linn (checked with online Flora of China (Li, 2007)) and (ii) they could share the same plant functional types from the modeling perspective (e.g., the terrestrial biosphere model like ED2 (Ma et al., 2022)). Other parameters pertaining to iHydroSlide3D v1.0 are listed in Table S1.

3.3. Model simplifications and limitations

The modeling framework facilitates the representation of key hydro-mechanical properties and processes on a catchment scale. The computational load of iHydroSlide3D v1.0 can escalate when more detailed supporting input information is provided. The simplifications were undertaken to align with the scope of our study, which concentrates on the long-term simulation of flood and landslide generation,

considering the dynamics of vegetation. These include the following:

- Homogeneity of climate variables across the region was assumed for simplicity, given the relatively small size and homogeneous characteristics of our catchment. This includes assuming homogeneous horizontal LAI and root cohesion, while disregarding the impact of vegetation density and interactions between neighbouring root systems (Schwarz et al., 2012). This assumption will be tested in Section 4.2.
- Factors affecting vegetation dynamics are simplified to temperature, vapor pressure deficit, and photoperiod. Other factors like water, nutrients, and specie competition are not considered.
- The discussion of vegetation was confined to a broad categorical level rather than an individual species level. A compromise was reached in the calibration of the root system, utilizing literature values.
- Since the study area is highly vegetated with minimal human intervention (Supporting Information S1), the anthropogenic activities such as deforestation and forest harvesting were not considered. Additionally, it was assumed that topographical characteristics remain constant during our long-term simulation, unaffected by anthropogenic activities or natural erosion.

The utilization of simplification facilitates the easier control and assessment of the added component within the distributed model. Nevertheless, such a simplification is not intended to demonstrate or exploit the distributed capabilities inherent in the model. Note that our model calibration and verification were conducted based on these assumptions (see in Supporting Information S1).

3.4. Computational scenarios and setup

The simulation encompasses the reproduction of historical events (refer to Supporting Information S1) and long-term modeling spanning from 2023 to 2122, covering a total duration of 100 years. To assess the impact of vegetation and its dynamics over this 100-years period, three computational scenarios were devised by differentiating the setup of vegetation conditions and outlined in Table 2: (i) a catchment with bare soil ("Bare"); (ii) a catchment with static, fully vegetated conditions ("S-Veg"); and (iii) a catchment with naturally dynamic, fully vegetated conditions ("D-Veg"). We specifically designed the S-Veg scenario to isolate it from natural dynamics, with vegetation status calculated as average values for the Day of the Year (DOY). As a result, the S-Veg scenario reflects only the average variations over the simulated period and does not exhibit inter-annual fluctuations. While iHydroSlide3D v1.0 employs the typical random-generation principle for failure depth (c_e), we manually introduced two additional fixed values of c_e, namely 1.5 m and 5 m, representing fully rooted (shallow) and partially rooted (deep) failures, respectively (as depicted in Fig. 1). This adjustment enhances the ability to compare the relationship between root structure and landslide depth.

To explicitly quantify and better analyze the contribution of vegetation and its dynamics to floods and landslides, we define several dimensionless indices by comparing the values of R_L and $Q_{\max}$ under preset scenarios:

$$\begin{aligned}
\Delta Q_{\max,\ \mathrm{Veg}} &= (Q_{\max,\ \mathrm{Bare}} - Q_{\max,\ \mathrm{D\text{-}Veg}})/Q_{\max,\ \mathrm{Bare}};\\
\Delta Q_{\max,\ \mathrm{VegDynamics}} &= (Q_{\max,\ \mathrm{S\text{-}Veg}} - Q_{\max,\ \mathrm{D\text{-}Veg}})/Q_{\max,\ \mathrm{S\text{-}Veg}};\\
\Delta R_{L,\ \mathrm{Veg}} &= (R_{L,\ \mathrm{Bare}} - R_{L,\ \mathrm{D\text{-}Veg}})/R_{L,\ \mathrm{Bare}};\\
\Delta R_{L,\ \mathrm{VegDynamics}} &= (R_{L,\ \mathrm{S\text{-}Veg}} - R_{L,\ \mathrm{D\text{-}Veg}})/R_{L,\ \mathrm{S\text{-}Veg}},
\end{aligned} \tag{11}$$

where the subscripts "Veg" and "VegDynamics" are used to distinguish between scenarios where vegetation is present (Bare vs. D-Veg) and where vegetation dynamics are considered (D-Veg vs. S-Veg). Note that these variables can assume either positive or negative values, indicating increased or decreased contributions to disaster events. Given the prohibitively extended simulated time required by the 3D manner in the landslide submodule at the catchment scale and over a long-term period, this study refrained from generating simultaneous outputs for hydrological and landslide variables. Instead, hydrological processes were simulated at a daily time step, while slope stability was assessed on the wettest day of each month, leveraging soil moisture as a key determinant. All hydrological variables were stored daily and prepared for the moment when the slope stability module is invoked. This arrangement ensures the computational feasibility of the study and captures essential variables that adeptly reflect the hybrid feedback of seasonal changes in vegetation. The whole simulation was executed at the DelftBlue supercomputing center (Centre, 2022), situated at Delft University of Technology.

Table 2
Computational scenarios.

Scenarios	Setup of LAI and root biomass over the 100-year simulation
Bare	The value of LAI is zero for all pixels and the root system is not considered ($c_r = 0$)
S-Veg	Average values of simulated LAI and root biomass for each DOY over a 100-year simulation
D-Veg	The daily LAI is simulated by the prognostic phenology model and the root biomass is simulated by the regression model

Note: Day of the Year (DOY) is a numerical representation of a specific day in the calendar year, starting from January 1st as DOY 1, and progressing sequentially through the year. For example, January 1st is DOY 1, March 1st is DOY 60 (in a non-leap year), and December 31st is DOY 365.

4. Results

4.1. Overview of simulation

The simulation results mainly include uncertainty analysis, model verification and computational scenarios analysis. The uncertainty analysis includes the rationality of the assumptions (or simplifications) of this study and their impact on the subsequent simulation results (Section 2). The model validation aimed at reproducing historical floods and landslides using the modified model (Section 3). To elucidate general hydrological and mechanical effects of vegetation under seasonal variations (in Section 4.4.4), we present a time series extracted from a comprehensive 100-year run, focusing specifically on a 5-year window (from 2031 to 2035). We then emphasize the impact of vegetation dynamics in Section 4.5. In 4.6, our presentation shifts to results derived from the entire simulation durations.

4.2. Uncertainty analysis

4.2.1. Homogeneity of vegetation assumption

Our simulation utilized the LAI data from the meteorological station to homogenize the vegetation conditions across the catchment, which introduced uncertainty. To evaluate this, we compared the spatial distribution differences between the homogeneous LAI and MODIS LAI observations across the catchment. To adequately capture the seasonal variability, we calculated the multi-year monthly averages of both the homogeneous LAI and MODIS LAI distributions (Fig. 4). The spatial distribution of MODIS LAI exhibits greater dispersion during the summer months, characterized by significant differences between extreme values, whereas the data are more clustered during the winter months. The homogeneous LAI consistently falls within the range represented by the box plots and follows a similar seasonal trend. In most months, the homogeneous LAI values closely align with the median of the MODIS LAI distribution, although they are slightly lower in June and July.

We further simulated and compared the daily evapotranspiration (ET) of the entire basin, accumulated from all cells, under the homogeneous assumption and the heterogeneous MODIS LAI scenario. The

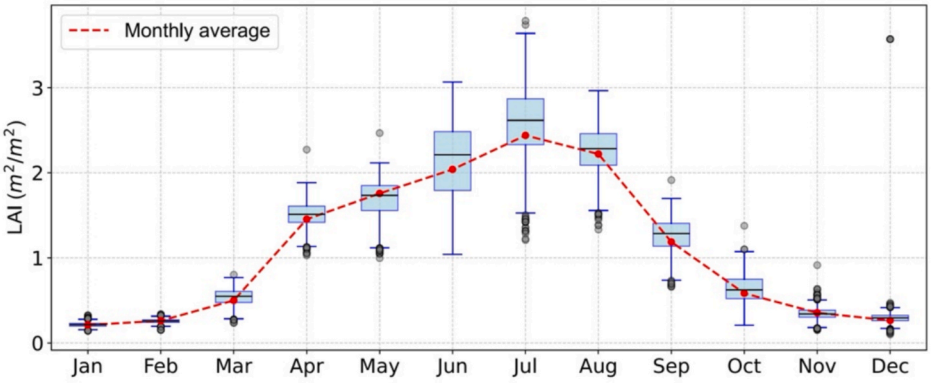

Fig. 4. Monthly variation of LAI from 2011 to 2021. Boxplots depict the distribution of heterogeneous MODIS LAI observations, while the red dashed line represents the monthly average for homogeneous vegetation. (For interpretation of the references to colour in this figure legend, the reader is referred to the web version of this article.)

overall trends of the two simulations are similar, with substantial overlap at many time moments (Fig. 5). However, at certain times, the homogeneous simulation results exceed those of the heterogeneous case. To better understand the extent to which this difference impacts the prediction of floods and landslides in this study, we constructed a semi-artificial case (see Fig. 6), where (a) the vegetation state was assigned to the moments of maximum ET difference, and (b) the rainfall input was set to the largest event in the subsequent 100-year series. We argue that such simulations effectively capture the relatively significant prediction uncertainty. Fig. 6 demonstrates that the assumption of vegetation homogeneity has minimal impact on flood simulations, whereas differences in slope stability are evident in the proportion of unstable areas within the region, which is less than 2 %. Thus, in all computational scenarios examined in this study, we assumed vegetation homogeneity.

4.2.2. Sensitivity analysis of the parameters

Fig. 7 presents a comprehensive overview of the computed sensitivity indices (S_I) for all calibrated parameters listed in Table S1. The analysis reveals that *coeR*, which represents channel flow parameters, exerts the most dominant influence on hydrologic runoff, followed by the overland flow speed parameters, *coeM* and *expM*. The impact of the interflow parameter coeS and the infiltration curve parameters (B) on runoff generation was relatively lower in comparison. The partitioning of water from overland and interflow reservoirs to discharge for a general cell, as characterized by *KS* and *KI*, exhibited minimal effects. In the context of the regional unstable area, hydrological parameters were observed to have a limited effect on slope stability calculations, with B being relatively more sensitive, as demonstrated in Fig. 7b. Among the parameters that constrain the geometry of potential landslides, c_e exhibited higher sensitivity owing to its direct relationship with landslide depth. The LAI dynamic parameter τ showed no significant impact on either flood or landslide generation. Similarly, the regression coefficients ($c_1 \sim c_4$) for B_g dynamics had no substantial effect on the simulation of unstable areas. Since all vegetation dynamic parameters were defined by input data, the results indicate that variations within 10 % do not significantly influence flood and landslide predictions. Although sampling density D_e is not directly relevant to the physical processes, it determines the convergence of the calculations and significantly affects the results regarding the overall stability of the region.

4.3. Model parameterization and validation

The improved iHydroSlide3D v1.0 underwent validation with particular emphasis on the incorporation of vegetation components. The objectives of model parameter selection are as follows: (1) to verify the simulation results of each module against observations or data sets, and (2) to assess the model ability to capture flood and landslide events, as well as the rationality of its simulations over long time series. All the simulating parameters are listed in Table S1. The root architecture, including root area, root number, and root force, was parameterized based on literature data (Fig. S2). Another validation was performed concerning the F_s values for an ideal semiellipsoid failure, benchmarked at various failure depths (Fig. S2). Comparative analyses were performed between 1D and 3D slope stability models to highlight the contribution of root reinforcement on the overall stability.

Subsequently, the predictive ability of the model was tested to reproduce a historical flood-landslide cascading event that occurred from September 18 to 19, 2011 (Figs. S3-S6). To evaluate the model's performance in flood prediction, we computed three statistical metrics: the Nash–Sutcliffe coefficient of efficiency (NSEC), the Pearson correlation coefficient (CC), and relative bias. For spatial landslide prediction, the %*LRclass* index (Tran et al., 2018; Chen et al., 2023) was adopted as the evaluation metric. Two scenarios were simulated: one with realistic vegetated soil conditions and another with hypothetical bare soil

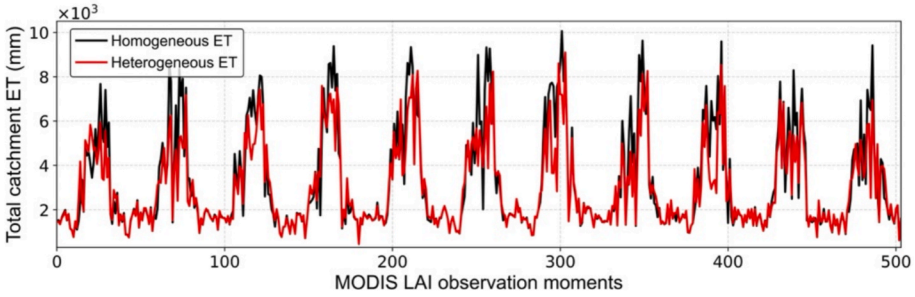

Fig. 5. Comparison of total catchment ET simulation at all MODIS LAI observation moments (8-day interval) under homogeneous and heterogeneous vegetation conditions.

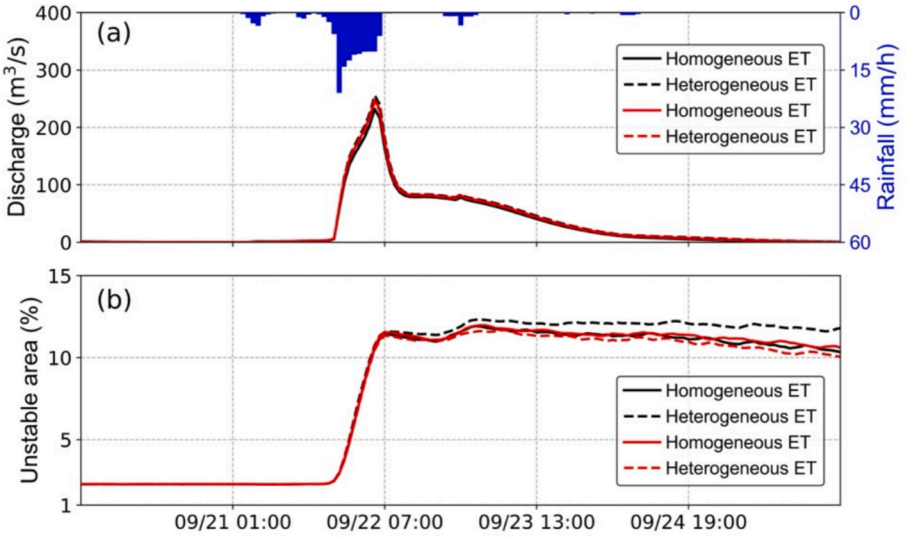

Fig. 6. Comparison of (a) flood discharge and (b) proportion of unstable area under extreme rainfall events for homogeneous and heterogeneous vegetation conditions. The vegetation state is chosen at the time of maximum ET difference: black represents 17 June 2016 (homogeneous ET > heterogeneous ET), and red represents 29 August 2019 (homogeneous ET < heterogeneous ET). The rainfall input corresponds to the largest event in the following 100-year series (from 19 September 2102, 18:00, to 26 September 2102, 02:00). (For interpretation of the references to colour in this figure legend, the reader is referred to the web version of this article.)

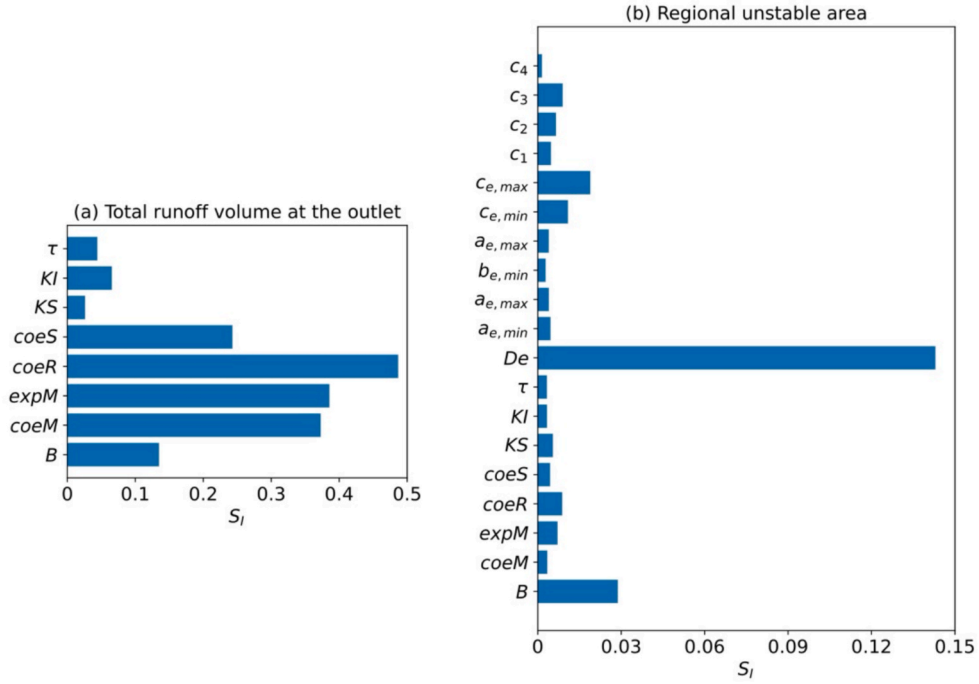

Fig. 7. Sensitivity analysis of the calibrated parameters in Table S1. The objectives are chosen as (a) runoff volume at the watershed outflow location and (b) regional unstable area.

conditions. The results indicate that while the difference in flood discharge between the two scenarios is minimal, the vegetated scenario demonstrates greater accuracy in predicting flood peaks (Fig. S3). In terms of spatial landslide prediction, the model achieved a higher % *LRclass* index score (92.56 % vs. 88.47 % in Table S2) when vegetation was taken into account.

Beyond event prediction, the model's performance was also evaluated over an extended time series. For the ecological submodule, the simulated leaf area index (LAI) and evapotranspiration (ET) time series were validated against MODIS datasets using Pearson's correlation coefficient (CC) and root mean squared error (RMSE). Fig. S7 demonstrates that the modeled LAI exhibits good agreement with observations, with CC = 0.84 and RMSE = 0.56. Similarly, the modeled ET also shows good agreement, with CC = 0.84 and RMSE = 16.63 (Fig. S8). Furthermore, the model was applied to simulate daily streamflow from 2010 to 2012. The dynamic-vegetation configuration demonstrates superior simulation accuracy compared to the bare configuration, as evidenced by improvements in all evaluated metrics: NSEC (0.73 vs. 0.86), CC (0.86 vs. 0.80), and bias (−14.6 % vs. 71.1 %). Our findings demonstrate that the improved iHydroSlide3D v1.0 in this work

exhibited superior performance in both event-specific and long-term predictions of flood and landslide occurrences. More detailed description (e.g., spatial patterns of soil moisture and factor of safety) can be found in Supporting Information S1.

4.4. General hydrological and mechanical effects of seasonal vegetation

4.4.1. Effect of vegetation on soil water balance

The precipitation followed the climate seasonality of alternating wet and dry seasons (Fig. 8a). The ET values depend on the climate variables and the modelled LAI. For D-Veg and S-Veg, strong seasonal variations of ET were observed in each generic year. The basin exhibited high ET in summer (can reach 4 mm) while a low ET rate (around 1 mm) was kept during fall and winter months (around from ~October to ~May) (Fig. 8b). For bare soil, ET rate was less than 2 mm most of the time, with no significant seasonal variations, even under favourable weather conditions in summer. In general, the presence of vegetation can greatly enhance ET during summer months. The vegetation dynamics only played an effective role (either growth or decay) in summer months, differing in specific ET values between D-Veg and S-Veg, while there was no obvious difference for all three scenarios during fall and winter months.

The soil moisture series (Fig. 8c) was strongly related to ET value, i.e., the annual occurrence of relatively wet or dry conditions can be clearly observed. The soil moisture significantly increased during the wet season, with fully saturated ($Sr = 1$) reached after intense rainfall. Comparison between the bare and vegetated (D-Veg and S-Veg) configurations obviously showed the enhanced water-loss effect contributed by vegetation in wet months, though this difference was less pronounced during dry seasons that show little precipitation and almost the same ET. Although soil moisture dynamics were not considerably impacted by vegetation dynamics, D-Veg and S-Veg nevertheless yields some different fluctuations due to ET differences.

Fig. 8d shows the modelled runoff was negligible during dry seasons, although some discharge fluctuations occurred at the early stage of wet seasons (around from ~April to ~May). The larger discharges were observed in summer seasons and some of them reaches the flood level (~50 m^3/s). Similar to soil moisture, the effect of vegetation on the runoff reduction was clearly present (Fig. 8d). Some slight differences can be observed between the scenarios of S-Veg and D-Veg. The results of spatial patterns of surface runoff at t_1 and t_2 (marked in Fig. 8) are depicted in Fig. 9. A general higher modelled discharge was observed for bare soil compared to S-Veg and D-Veg, and this difference was more apparent at the catchment outlet (inset map in Fig. 9). A similar difference also exists between D-Veg and S-Veg, suggesting a decay trend at t_1 and a growth trend at t_2, respectively, which resulted in opposing effects.

4.4.2. Effect of vegetation on slope stability

The results of regional slope stability were analysed in terms of percent area computed as unstable and various exceeding failure probabilities. Fig. 10a shows the evolution of the percentage of unstable area for three scenarios with c_e of 1.5 m (fully rooted landslides) and 5 m (partially rooted slopes). The curves show a similar seasonality as the soil moisture content results; the minimum values were more steadily maintained during the dry seasons. The unstable area for the bare soil, in the absence of vegetation cover, not only showed a high peak value of around 15 % but also exhibited a drastic increasing trend during the soil wetting up (maximum difference reaches around 10 %). The increasing behaviour of unstable area for bare soil started earlier (from May) during wet seasons, and a similar behaviour of receding was observed for all scenarios. As a result, the landslide-prone period for D-Veg and S-Veg scenarios lasted shorter. The differences between the D-Veg and S-Veg scenarios occurred before as well as after the peak state (Fig. 10a).

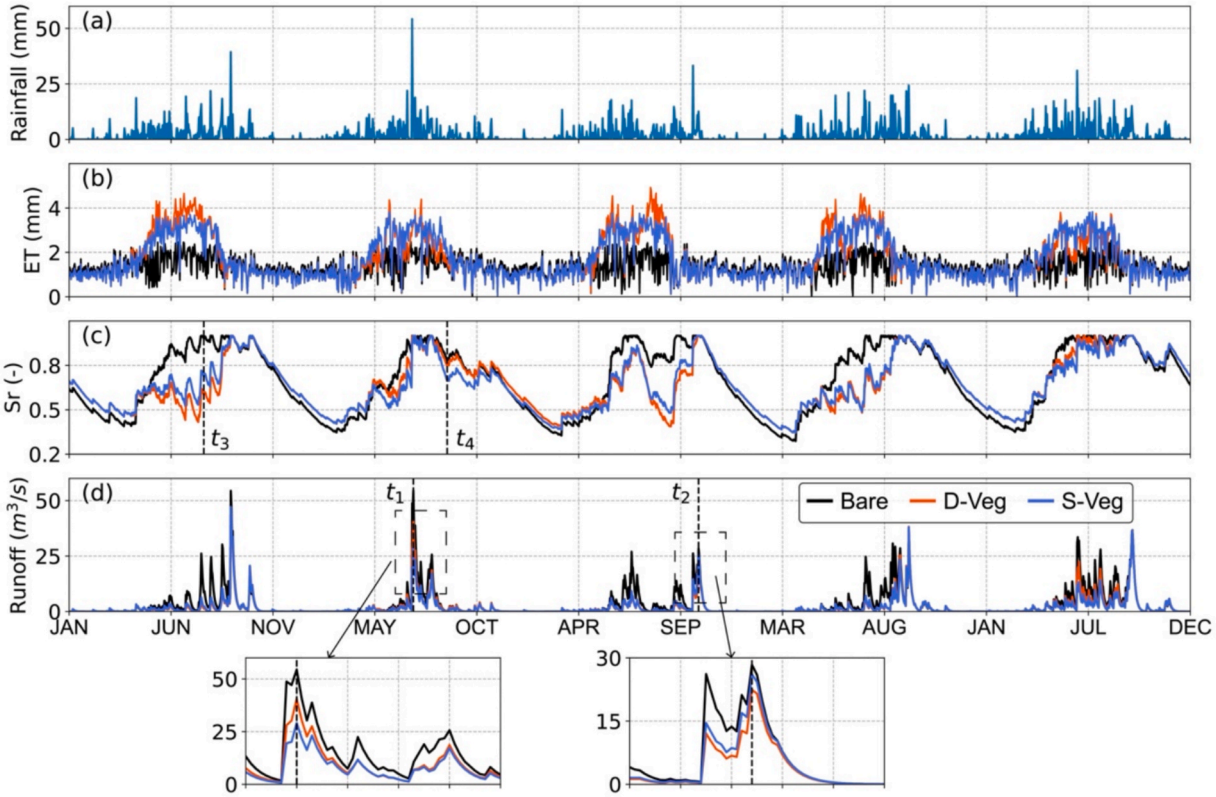

Fig. 8. A five-year time series (2031 ~ 2035) of (a) precipitation, (b) evapotranspiration, (c) regional average soil moisture, and (d) runoff at the basin outlet. Results for three scenarios (Bare, D-Veg, and S-Veg) are plotted at daily scale for comparison. t_1, t_2, t_3, and t_4 are chosen moments to show spatial patterns for the following analysis.

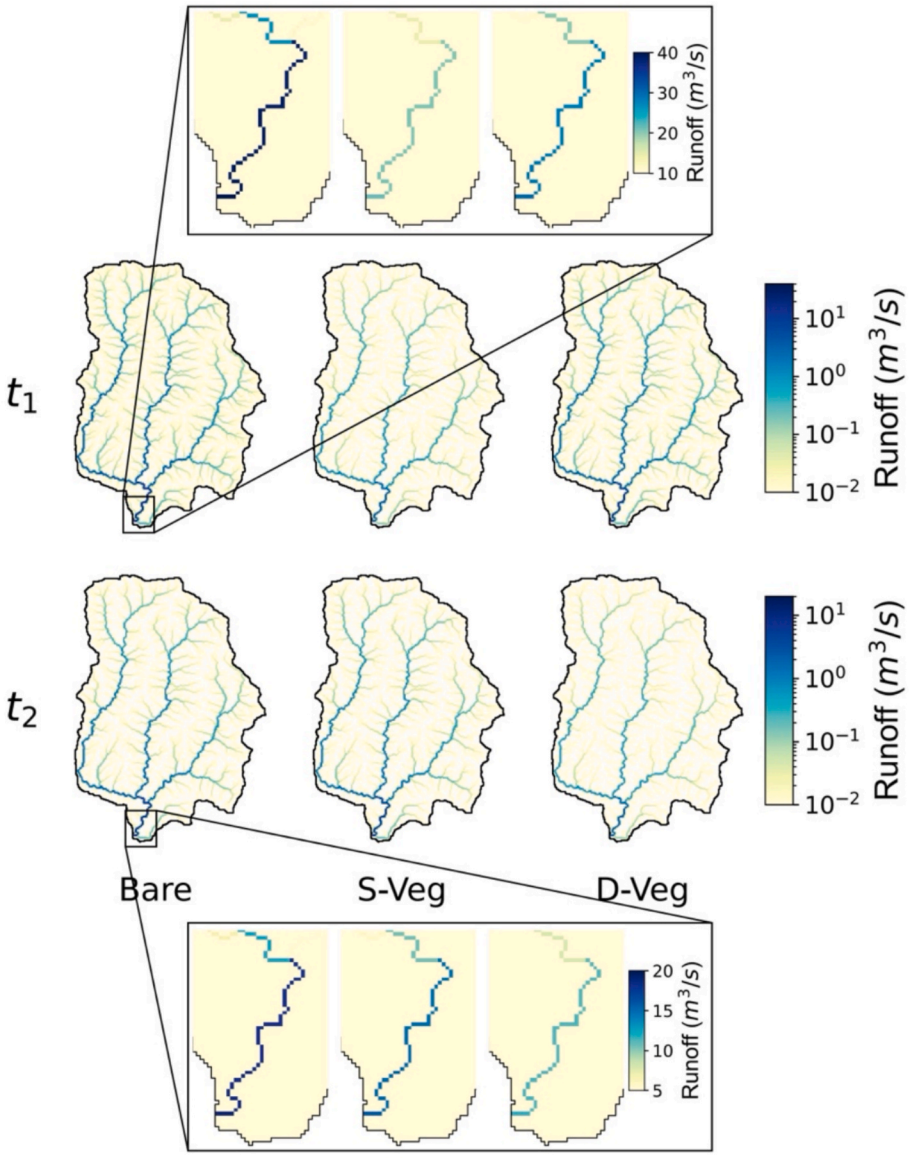

Fig. 9. Spatial patterns of surface runoff for three scenarios at t_1 and t_2 picked in Fig. 4d. The inset map zooms in on the catchment outlet, showing the values along the discharge channel for both time points.

However, the differences in unstable area between D-Veg and S-Veg scenarios was much less pronounced, even invisible (e.g., the fourth year in Fig. 10a).

A comparison among the three scenarios (Fig. 11) clearly highlights the vegetation effect and its dynamics on regional slope stability in terms of the distribution of potentially unstable areas. For both typical moments (t_3 and t_4 in Fig. 8c), the vegetation provided a positive effect on landslide-hazard reduction, particularly at t_3 when the modelled unstable area under the bare soil scenario was larger due to the absence of root reinforcement. The comparison between D-Veg and S-veg indicates in Fig. 11 at t_3 and t_4 explicitly showed that the effects of vegetation dynamics could be either positive or negative, which enhanced the soil stability at t_3 and had less protection at t_4.

Random generating the landslide depth (c_e) value from 1.5 m to 5 m only makes a negligible difference in the case of bare soil, while it turns out to be more significant for D-Veg and S-Veg during the wet season. The reduction of unstable area of the region reached its maximum during summer seasons, while the smaller effect is still maintained during dry periods. The vegetation dynamics did not show large differences in the percentage of unstable areas since behaviours of unstable area fluctuations are almost identical for D-Veg and S-Veg (Fig. 10a). The results provided by employing random c_e (Fig. 12a) inherit all characteristics of the three scenarios presented in Fig. 10a except the percentage values of D-Veg and S-Veg, which fall between those from 1.5-m and 5-m cases (Fig. 10a).

The time-series results of the percent area with various P_f (Figs. 10b-d and 12b-d) are similar to the unstable-area curve (Figs. 10a and 12a) for all scenarios with reductions in values. Both random and fixed values of c_e in Figs. 10 and 12 indicate that the P_f area is more sensitive to the landslide depth for S-Veg and D-Veg, which is less pronounced for bare soil. Moreover, like the unstable area, the specific values of P_f area estimated by using the random c_e also fell between those from cases of fixed c_e.

4.5. *Effect of vegetation dynamics on floods and landslides*

To emphasize the impact of vegetation dynamics, we present periods when significant vegetation growth or decay can be observed (Fig. 13). These durations are defined as the 15 days before and after the maximum difference in the LAI between the D-Veg and S-Veg scenarios.

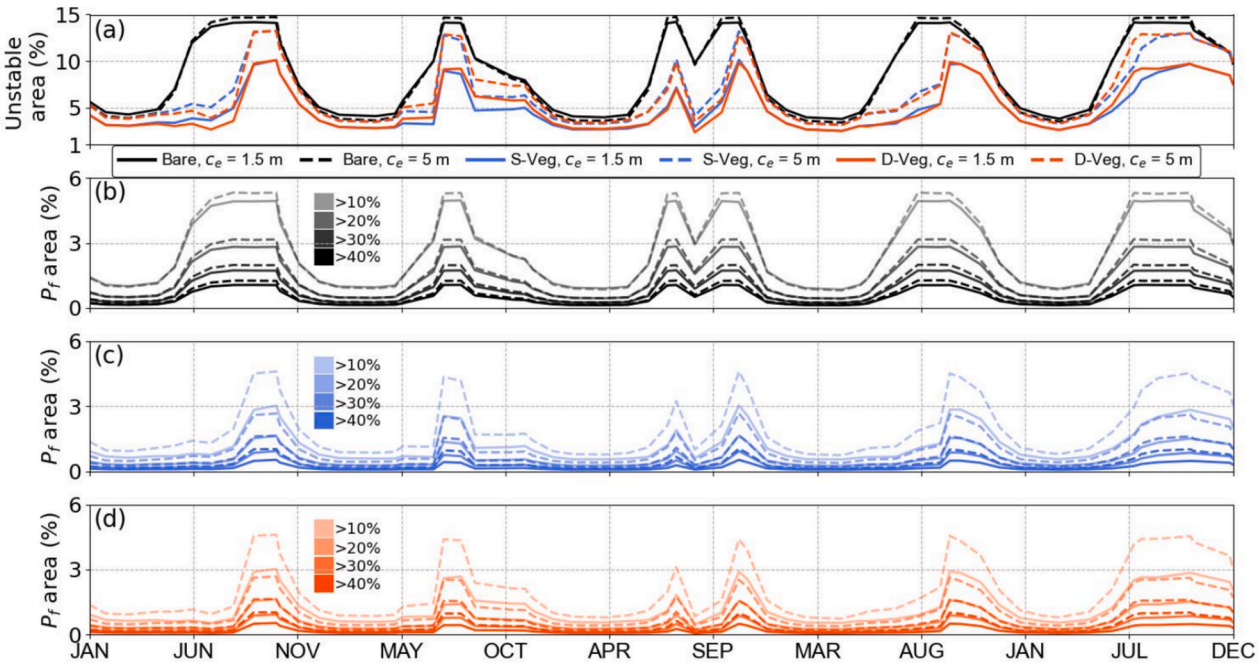

Fig. 10. A five-year time series of the percentage of (a) unstable areas for three scenarios with certain failure depth (c_e) values (1.5 m and 5 m), and (b) ~ (d) are computed as various failure probabilities (P_f) with certain c_e values for Bare, D-Veg, and S-Veg, respectively.

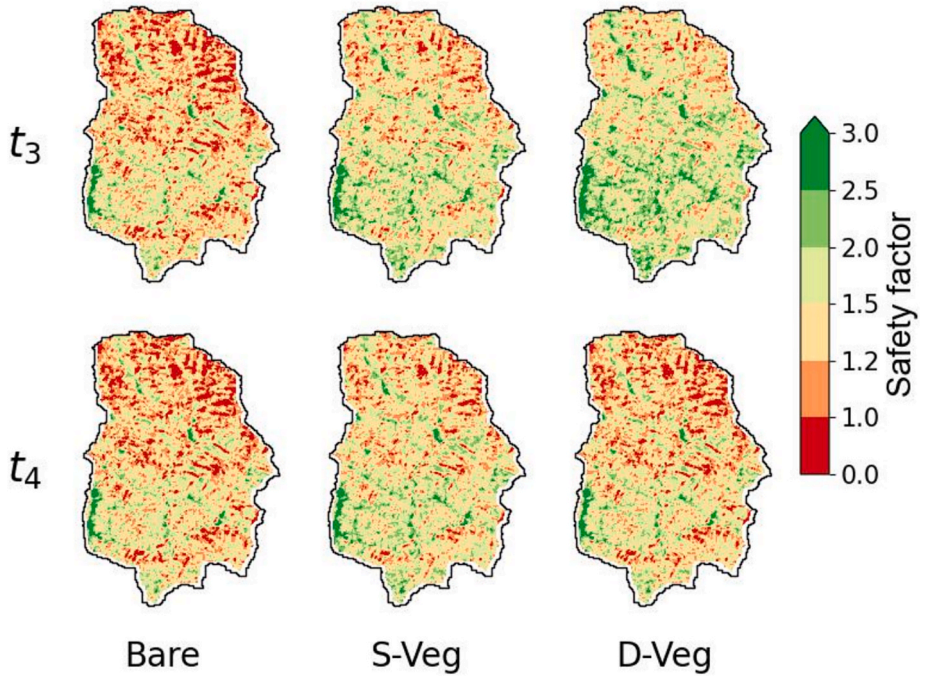

Fig. 11. Spatial patterns of safety factor (F_s) for three scenarios at t_3 and t_4 picked in Fig. 8c.

This time frame is also suitable for observing flood and landslide events driven by rainfall. Fig. 13a and b depict the trends of vegetation growth and decay, respectively. As shown, the ET rate for the D-Veg growth scenario is notably higher than that of the S-Veg scenario (Fig. 13c and d), with bare soil following in the ranking. Conversely, during the decay phase, the ET rate for D-Veg is significantly lower than that of S-Veg, approaching the rate observed in the bare soil scenario (Fig. 13d).

During rainfall events, flood discharge is reduced by both D-Veg and S-Veg in both growth and decay phases (Fig. 13e and f). However, this effect is less pronounced for D-Veg during decay because the difference between its ET rate and that of bare soil is minimal (Fig. 13d). The disparity in flood discharge between D-Veg and S-Veg further illustrates vegetation dynamics, with the difference being more noticeable during the decay phase. It is important to note that during the wetting phase, early rainfall events do not produce a significant gap in flood discharge, whereas later rainfall events show a more pronounced effect.

Regarding landslides, the simulation results reveal more pronounced differences among the three scenarios compared to flood discharge (Fig. 13g and h). Regardless of vegetation growth or decay, soil stability in both D-Veg and S-Veg scenarios is superior to that in the bare

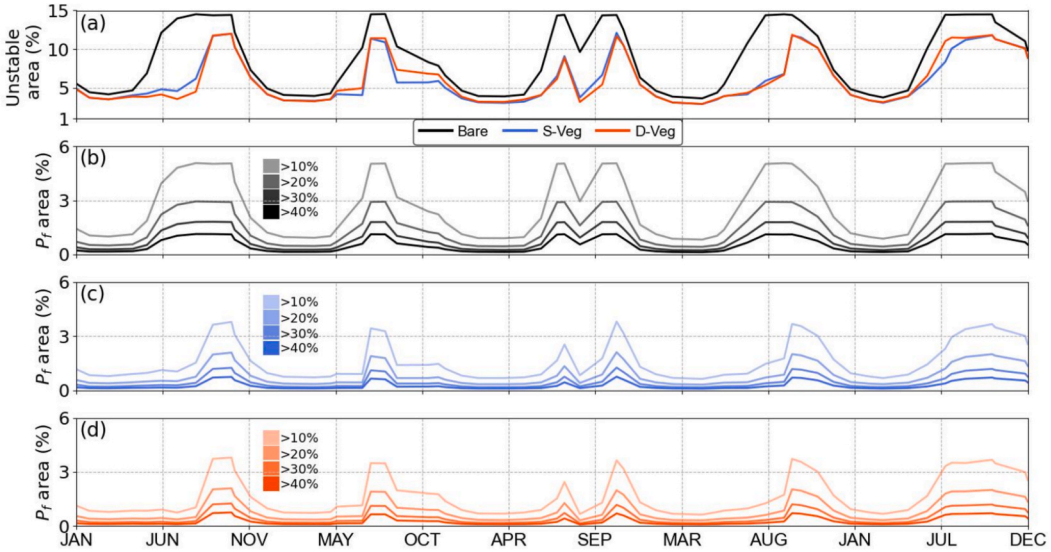

Fig. 12. A five-year time series of percentage of (a) unstable area for three scenarios with random failure depth (c_e) values (ranges from 0.5 to 5 m), and (b) ~ (d) are computed as various failure probabilities (P_f) with random c_e values for Bare, D-Veg, and S-Veg, respectively.

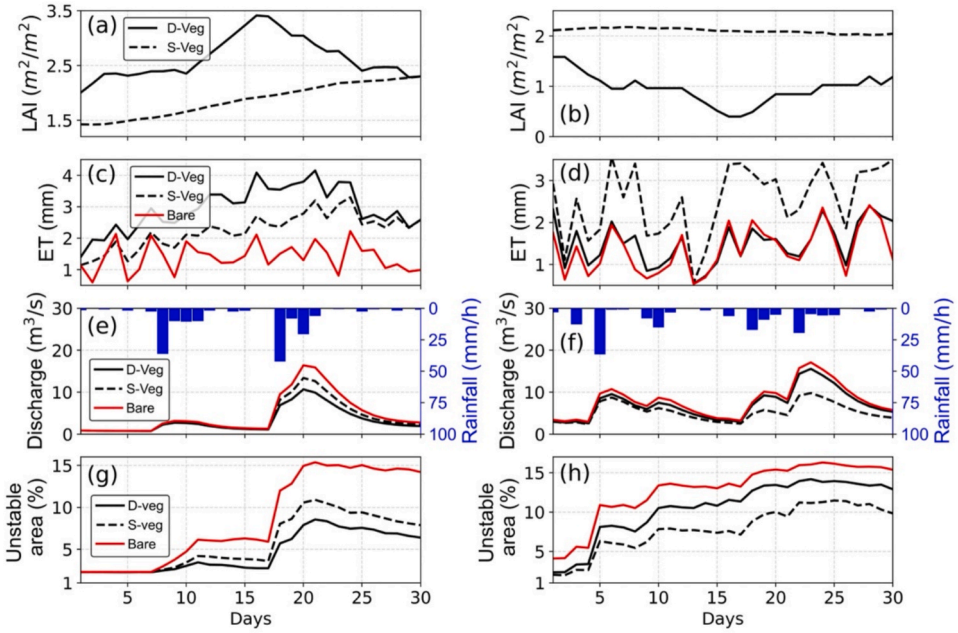

Fig. 13. Durations of apparent vegetation growth (left column, April 19, 2034, to June 8, 2034) and decay (right column, July 6, 2115, to August 25, 2115) and their effects on (a, b) LAI, (c, d) ET, (e, f) flood discharge, and (g, h) the proportion of unstable areas.

scenario, with the benefits being more significant during the growth phase. In rainfall events, soil stability is strongly influenced by vegetation dynamics (evidenced by yields of Veg and S-Veg). Even when ET rates are similar, soil stability in the D-Veg scenario remains superior to that in bare soil (Fig. 13h), due to the mechanical reinforcement provided by the root system.

In addition to examining local events, we further extend the analysis to encompass the entire simulation sequence. As shown in Fig. 14a, the vegetation dynamics of the LAI was modeled in the D-Veg scenario (shown as annual mean), and the static values were also provided by S-Veg as a constant (equal to 1.068 m^2/m^2 without inter-annual variations). By comparing them, we defined three representative years for D-Veg series: (i) average year (yr_1 = 47, annual LAI = 1.073 m^2/m^2): the vegetative state is very close to the static one; (ii) growth year (yr_2 = 71, annual LAI = 1.268 m^2/m^2): the vegetation has a significant growth trend; (iii) decay year (yr_3 = 84, annual LAI = 0.857 m^2/m^2): the vegetation has a significant decay trend.

The daily simulated runoff was analysed for three corresponding years (Fig. 14b–d) by calculating the exceedance probability (flow duration curve). For the average year (Fig. 14b), the results of D-Veg and S-Veg almost overlap for all probabilities. The difference between the bare and vegetated cases was mainly observed in the range of $0 < P_{exceedance} < 0.5$, which is further shown as the convergence at the higher discharges. Fig. 14c clearly highlights both effects of vegetation and vegetation dynamics on flood peak reduction in the growth year. The lower flood magnitude was observed from D-Veg for a given flood frequency (around $P_{exceedance} < 0.7$) than that from Bare and S-Veg or, alternatively, a lower return period for a given flood magnitude. The exceedance curve of S-Veg fell between those from Bare and D-Veg while, three curves converged at the extremely large flow (> 150m^3/s)

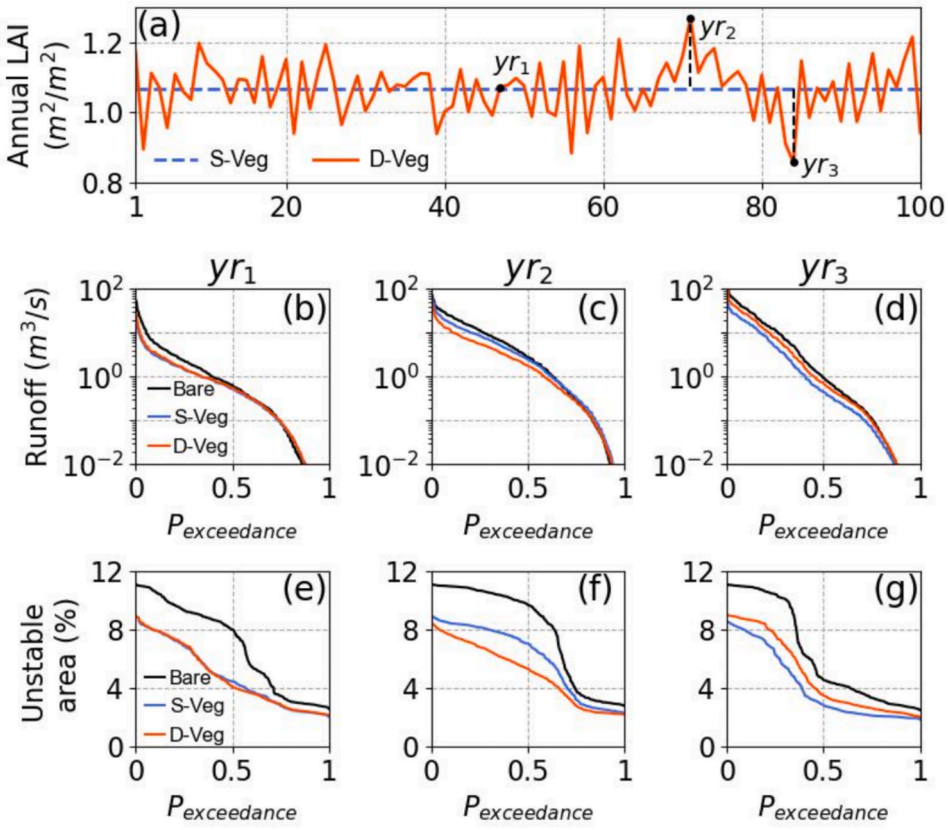

Fig. 14. Annual series of LAI in the 100 years (2023 ~ 2122) are plotted in (a). The marked points (yr_1, yr_2, and yr_3) are three representative years defined as average, growth, and decay year, respectively. (b) ~ (d) and (e) ~ (g) are exceedance probabilities for runoffs and percentages of the unstable area in yr_1, yr_2, and yr_3, respectively.

and low discharge close to zero (Fig. 14c). The lower discharge from D-Veg and S-Veg in the decay year occurred in a larger range of $P_{exceedance}$ (Fig. 14d). The behavior of D-Veg and S-Veg, however, resulted in the opposite regarding the effect of vegetation growth and decay.

Fig. 14e–g shows the frequency curves of the unstable area. For all the representative years, a lower percentage was calculated from D-Veg and S-Veg than that from Bare for any given frequency. Apparent visual convergence (or convergent trend) was observed in average and growth years for the small to moderate landslide events, while there were still differences in the decay year. Similar to the flood frequency curve in Fig. 14b, no visual difference between D-Veg and S-Veg was found for unstable areas in the average year. Such a difference clearly appeared in the growth (Fig. 14e) and decay year (Fig. 14g). In particular, the effect on unstable-area reduction was more pronounced in the growth year and less pronounced in the decay year, while the opposite relationship between them was also clearly depicted.

4.6. Long-term hazard analysis of floods and landslides

The annual peak discharges (Q_{max}) and landslide hazards (R_L) were calculated using the method provided in Section 2.3. The results for three scenarios were ranked by exceedance probability (Fig. 15). For the low to moderate events of the flood, the vegetation significantly moderated the flood, which declined gradually with an increasing flood magnitude (Fig. 15a). The apparent convergence was observed at extremely large discharges (> 150m^3/s), where the vegetation cover

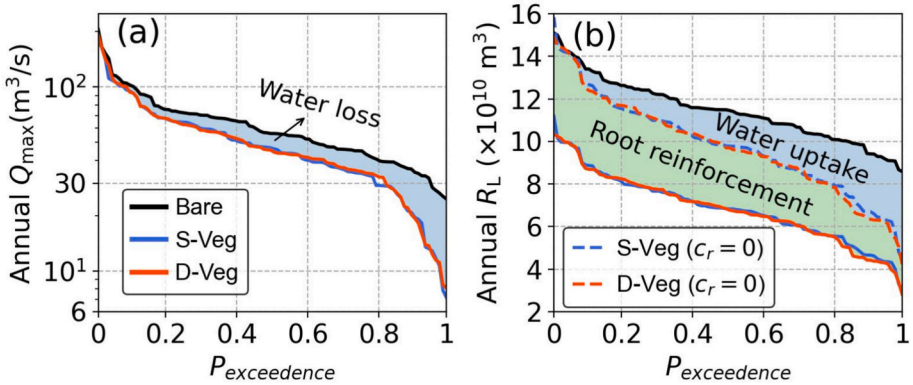

Fig. 15. Exceedance probabilities of (a) annual peak flow and (b) annual landslide hazard, for three scenarios over a 100-year period. The shaded areas depict the contributions of vegetation effects compared to the bare soil.

had little (or no) impact. No pronounced evidence pointed out an effect of vegetation dynamics (almost overlapping curves of D-Veg and S-Veg).

Fig. 15b shows the comparisons of annual landslide hazards obtained for all scenarios. To compare and distinguish the individual components (water uptake and root reinforcement) of the compound effect of vegetation on landslide hazard mitigation, we manually set root cohesion to zero while retaining vegetation evapotranspiration. It should be noted that this scenario does not represent a real-world situation (and differs from the Bare, D-Veg, and S-Veg scenarios) but is a numerical experiment designed solely for analytical purposes. For the original D-Veg and S-Veg, the vegetation reduced the annual landslide hazards for any given probability and the influence slightly declined for larger events. The results of additional cases fell between the bare and vegetated cases with $c_r > 0$. It is worth noting that clear convergence was observed with increasing annual landslide hazard, like the curves for annual Q_{max} (Fig. 15a). These differences helped to distinguish the components (water uptake and root reinforcement) in the compound effect of vegetation on landslide hazards moderation, which taking the fractions of 46.3 % and 53.7 %, respectively.

The annual peak flow and landslide hazard were further assessed using Eq. (11) and the time series of $\Delta Q_{\max}$ and ΔR_L were calculated for both vegetation and vegetation dynamics, respectively (Fig. 16). The vegetation effect on hazards reduction was positive for both flood and landslide events ($\Delta Q_{\max,\,Veg} > 0$, $\Delta R_{L,\,Veg} > 0$), which was more pronounced in slope-stability modeling than runoff. A strong variability was observed for $\Delta Q_{max,\,Veg}$, with the maximum value exceeding 0.5 and the minimum value is close to zero (Fig. 16a). The values of $\Delta R_{L,\,Veg}$ was greater than zero for each year, indicating a relatively steady positive effect was obtained for long-term landslide prevention. The contributions of vegetation dynamics depended on the natural evolution of plants (grow or decay) and showed much less pronounced gains than those of pure vegetation. The fluctuations of them could be interpreted from the results of the annual LAI (Fig. 14a) that represented the vegetation dynamics in this work.

5. Discussion

5.1. Modeling framework

This study proposed a comprehensive modeling framework designed for catchment-scale and long-term assessment of flood and landslide responses to dynamic vegetation. The model updated the iHydroSlide3D v1.0 (Chen et al., 2023) by incorporating vegetation components, specifically the LAI, root characteristics, and their seasonal dynamics. In the hydrological module, similar functionalities to numerous eco-hydrological models (Donohue et al., 2010; Bellot and Chirino, 2013; Parr et al., 2015) are implemented, wherein ET is calculated based on modeled or remote-sensing LAI. The landslide module incorporates the RBMw, enabling the consideration of both basal and lateral reinforcement of the root system across all discrete slide surface elements. The use of RBMw method is specific to each root fiber and is not limited by the complexity of the root structure, provided sufficient observational data are available. In contrast to the limitations of the simple infinite model in representing lateral reinforcement (Arnone et al., 2016; Hales and Miniat, 2017; Lann et al., 2024), our results demonstrate significant improvement through the combination of higher dimensions of landslides and a more intricate root structure. Compared to analogous methods that integrate the 3D stability model and FBM/RBM, such as MD-STAB (Cislaghi et al., 2017; Cislaghi et al., 2018) and r.slope.stability (Schmaltz and Mergili, 2018), our proposed modeling framework offers the advantage of coupling more comprehensive hydrological processes and vegetation dynamics. These features fill a crucial gap in existing tools, potentially contributing to the comprehensive assessment within vegetated catchments where flood and landslide hazards coexist.

5.2. Hydrological and mechanical effects of vegetation on floods and landslides generation

The hydrological effect of vegetation mainly referred to the ET simulation in this study (Ng et al., 2015; Parr et al., 2015; Arnone et al., 2016). The seasonal variability of LAI indicated that the vegetation could dominate the ET process in the summer seasons due to the beneficial weather conditions for plant growth. The daily ET for bare soil also increased in summer but was significantly underestimated due to the absence of vegetation. The modeling soil moisture was corroborated to be strongly related to ET values serving as forcing data. The pronounced effect on soil water balance happens when (i) the vegetation dominates the ET process and (ii) the soil is unsaturated and slowly wets up (i.e., no extraordinary precipitation event). The enhanced evapotranspiration by the vegetation reduces the antecedent soil moisture for the subsequent runoff generation modeling. However, during large rainfall events, the volume of water may exceed the absorption and management capacity of both the soil (loam and clay loam in this region) and vegetation. Once the soil becomes saturated or the rainfall intensity surpasses the infiltration rate, the ability of vegetation to mitigate runoff is significantly reduced. Consequently, excess water is more likely to run off, regardless of the extent of vegetation cover. While loam soils are more permeable and can manage rainfall more efficiently, clay loam soils, due to their lower permeability, may saturate more quickly, leading to increased runoff. In both cases, once a certain threshold of rainfall intensity is reached, the soil's physical properties—particularly its permeability and water retention capacity—become more influential than vegetation

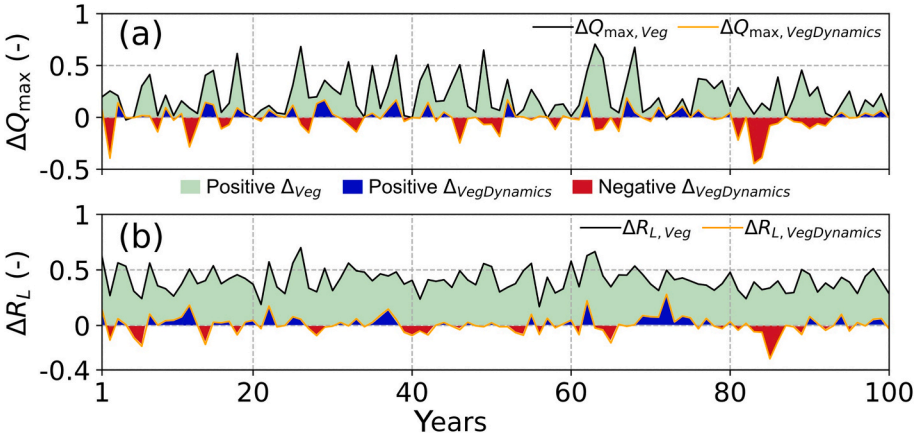

Fig. 16. Time series of contributions of vegetation and its dynamics in (a) annual peak flow and (b) annual landslide hazard over a 100-year period. The shaded areas depict the positive or negative contributions of vegetation and its dynamics.

alone in controlling runoff and flooding. Moreover, steeper slopes increase the velocity of surface runoff, further limiting the ability of vegetation to retain water and potentially outweighing its effects in controlling flooding during large rainfall events. This result agrees with the available field experiment (Zhang et al., 2014), where the runoff amount gap narrows as rainfall intensifies. Similar numerical results were also reported that the difference between bare and vegetated configurations are less visible during the wet period with relatively high soil moisture (Arnone et al., 2016).

The mechanical root reinforcement was evaluated by calculating the regional unstable area and failure probability. Employing the 3D slope stability model provides a comprehensive F_s for a potential failure by describing its geometry (Mergili et al., 2014), rather than calculating the F_s along the soil depth (e.g., the results by Ng et al. (2015) and Arnone et al. (2016)). This study also differs from the synthetic work (Schmaltz and Mergili, 2018) that used the critical length of the slip surface. Instead, the landslide size (length, width, and depth) was randomly generated within the input ranges. The ratio of length to depth still guarantees that the dimension follows the shallow criterion (Mergili et al., 2014). However, the landslide depth (could reach 5 m as the maximum) in this study well represents the deeper failures that are partially reinforced by the shallow roots, while most studies are limited to a depth fully rooted (normally < 2 m) (Ng et al., 2015; Liu et al., 2016; Arnone et al., 2016; Feng et al., 2020). The reduction of and F_s and P_f in this work well demonstrated the common view that both the hydrological and mechanical effects of vegetation can benefit soil stability (Chirico et al., 2013; Arnone et al., 2016). The modeling yields with the certain c_e (1.5 m and 5 m) also concur with Schmaltz and Mergili (2018) who suggested that the relation between soil thickness and the root profile morphology should be under particular consideration. Moreover, our results indicate that the deeper landslides (e.g., 5-m c_e) are still stabilized by vegetation in the absence of the hydrological effect, though the gain could only be ~1 % in terms of the unstable area. This could be pronounced for landslide disaster prevention since the P_f generally reaches its peak at that moment and the magnitude is also probably huge, especially for a long duration (i.e., estimated by Eq. (9)). Our results further suggest that the root system apparently increase the model uncertainty since the c_e is randomly generated, which, in turn, requires more computation to converge, if the family of depth-searching methods are used (e.g., r.slope.stability (Schmaltz and Mergili, 2018)).

5.3. Vegetation growth and decay dynamics

Studies on hydrological-geotechnical modeling that focus on vegetation effects rarely consider the dynamic vegetation. (Ng et al., 2015; Arnone et al., 2016; Schmaltz and Mergili, 2018). In this work, the dynamics of vegetation are aligned with seasonal changes in LAI and focus solely on key drivers of vegetation. A more realistic approach could incorporate factors such as soil moisture, nutrient availability, CO_2 concentration, and biotic interactions (e.g., competition, herbivory) (García-Gamero et al., 2021; Jin et al., 2021). However, the simplified method employed here prioritizes practicality and aligns with data availability, as the required input variables are relatively easy to measure. Additionally, LAI is widely used in vegetation studies and facilitates model validation and calibration (Savoy and Mackay, 2015).

Our findings reveal that vegetation dynamics can both strengthen and weaken the overall effect of vegetation compared to static conditions. These results imply that since vegetation dynamics significantly influence the magnitude of both floods and landslides, they should be carefully considered during periods with pronounced vegetation growth or decay. Unless vegetation dynamics follow a consistent annual cycle (e.g., as in the case of yr_1), which is rare in reality, neglecting this influence may lead to inaccurate assessments of disaster risks (Sheng et al., 2022). Considering the dynamics has also been regarded as an effective effort to help improve hydrological modeling for future predictions (Parr et al., 2015; Zhang et al., 2019b).

5.4. Annual flood and landslide hazards

Compared to the daily series, the annual disasters offer a more comprehensive perspective, encompassing events that are relatively large in scale and of significant concern. The proposed assessment method (in Section 2.3) for landslides takes advantage of considering the wet season duration, occurrence probability, and landslides magnitude. This results in distinct values of R_L for each year. In this study, vegetation has proven to be effective in mitigating annual landslide hazards across events with varying frequencies. Furthermore, the positive impact of vegetation on soil stability is more pronounced when compared to its effect on annual floods. This is attributed to the continuous reinforcement provided by the root system, even after the slope has reached a fully saturated state. For the annual Q_{max}, our results visually demonstrate that these effects are more pronounced in small to moderate events and diminish in larger events. This pattern aligns with Bathurst et al. (2020) and is consistent with Calder et al. (2007), who asserted the absence of significant benefits of forests for larger rainfall events. In these substantial events, the impact of soil moisture deficit on discharge generation is minimal. A similar pattern emerges in our auxiliary modeling setup ($c_r = 0$, i.e., without mechanical reinforcement), further supporting the notion that the hydrological effect of vegetation may be negligible in very large events. This approach effectively disentangles the contributions of hydrological and mechanical effects (46.3 % versus 53.7 % in this study) to landslide hazard reduction over the long term. Comparable methodologies were employed in F_s estimation, considering solely mechanical reinforcement and exclusively the hydrological reinforcement effect (Bordoni et al., 2024). Our results suggest that mechanical reinforcement exerts a more substantial effect, aligning with the findings of Bordoni et al. (2020) (with higher root density) and field experimental observations (Zhang et al., 2014). However, this conclusion contradicts the perspective of Arnone et al. (2016), who argued that the effect of root water uptake outweighs mechanical reinforcement. Nevertheless, uncertainties persist, acknowledging that this relationship is highly contingent on factors such as region, plant species, and climate patterns. Given the absence of substantial climate trends, vegetation dynamics have little impact on Q_{max} and R_L. The long-term simulation, encompassing growth and decay years, may exert a modest influence on frequency patterns. Our findings, however, underscore the importance of considering vegetation dynamics in specific years when positive or negative effects are more noticeable.

5.5. Limitations and future work

The assumption of vegetation homogeneity in this study limits the ability to explore spatial heterogeneity in greater depth. The practical applicability of this study is more suited to small catchments with homogeneous characteristics. Vegetation heterogeneity can significantly influence the spatial variability of infiltration, runoff, and ET patterns, thereby affecting overall hydrological processes (Luan et al., 2022). Moreover, the mechanical reinforcement provided by roots varies with species, age, and density (Bordoni et al., 2024), which in turn affects the stabilizing role of vegetation. Additionally, the homogeneous assumption may fail to capture species-specific responses to environmental stressors, such as drought and flooding, or account for the evolution of vegetation patterns over time due to natural succession (Xu et al., 2016; Bayle et al., 2023). These broader, more realistic natural conditions could be better addressed by integrating more sophisticated terrestrial biosphere models, such as the ED2 model (Zhang et al., 2019a). Another limitation of this study is the exclusion of long-term topographic changes caused by erosion and sediment deposition. Such changes can alter slope geometry, drainage patterns, and soil properties, all of which are critical for hydrological processes and soil stability (Stephens et al.,

2021). Furthermore, the feedback between topography and vegetation dynamics (Huo and Sun, 2021) could introduce additional uncertainty into the results and pose challenges for parameter calibration.

The assumption of a relatively stable meteorological cycle in this study may not fully capture the variability and potential changes in climate conditions. Climate change and natural climate variability can significantly alter precipitation patterns, temperature regimes, and the frequency of extreme weather events, all of which have profound implications for flood and landslide hazards (Wasko et al., 2021). For example, increased rainfall intensity and prolonged droughts can affect soil moisture, vegetation health, and slope stability, leading to higher risks of hazards. Additionally, shifts in seasonal precipitation and temperature trends can alter long-term vegetation dynamics and hydrological processes (Huo and Sun, 2021).

The proposed framework represents an advancement in the field of eco-hydro-geotechnical modeling. Its modular design allows for the incorporation of alternative ecological models, providing versatility and adaptability. Key variables related to vegetation dynamics are parameterized in a way that allows them to be tailored to specific vegetation types and soil properties. To apply the model in regions with different climates, users would need to integrate site-specific climatic data and future climate projections to capture regional hydrological responses accurately. We particularly underscore the critical role of the root system in future research, as evidenced by the root cohesion values calculated in this study, reaching a maximum of ~15 kPa (consistent with literature values of 5–100 kPa for deciduous trees, as reported by Schmaltz and Mergili (2018)). The model also holds practical utility and can be employed as a valuable tool in various applications, such as revegetation projects like the "Grain for Green Project" on China's Loess Plateau (Zhang et al., 2022a) or in land preparation techniques (Yu et al., 2019). The methods and quantitative analyses presented in this framework offer valuable insights, particularly for areas prone to floods and landslides at the catchment scale. Integrating ecological restoration with sustainable land-use planning, supported by strong policy frameworks and community engagement, can lead to more effective and sustainable disaster mitigation outcomes (Han et al., 2021). Moreover, the framework holds promise in linking with future climate simulations, including Representative Concentration Pathway (RCP) scenarios (Vuuren et al., 2011). By accounting for climate-driven changes, the model can predict shifts in vegetation growth patterns. This integration could contribute to evaluating nature-based solutions for reducing and managing hydro-meteorological risks (Kumar et al., 2021). Recent findings suggest that revegetation has the potential to enhance land–atmosphere interactions, leading to increased precipitation (Zhang et al., 2022a). Vegetation acts as a feedback mechanism by influencing local climates, potentially mitigating some climate impacts (e.g., reducing temperature extremes, increasing soil moisture), but may be overwhelmed by extreme weather events (Zhang et al., 2021). Restoration efforts might face challenges from extreme weather such as droughts or heavy rainfall, potentially reducing their ability to manage flood or landslide hazards. Future work involves incorporating vegetation-climate feedback, enabling the study of trade-offs between vegetation restoration and natural disaster mitigation.

6. Conclusions

This study presents an improved hydrological-geotechnical framework for combined flood and landslide hazard assessment by integrating vegetation dynamics. The embedded vegetation growth module was employed to quantify the vegetation dynamics in terms of the LAI and root biomass. The model framework was tested here as a tool to quantify the long-term effects of vegetation on regional hydrological processes and slope stability. The modeling outcomes emphasize the substantial effect of vegetation on reducing soil moisture and streamflow during wet seasons, attributed to the elevated ET rate. Conversely, during dry seasons, the hydrological impact of vegetation is comparatively diminished, owing to the marginal divergence in ET values between bare and vegetated scenarios. Soil stability benefits from both the mechanical root reinforcement and reduction in soil moisture, leading to a significant decrease in the regional unstable area and the probability of landslides with various failure depths. The analysis of annual peak discharges and landslide hazards suggests that, while vegetation explicitly mitigates landslide hazards, it only attenuates flooding discharge for low to moderate events but not for large ones. The dynamics of vegetation play a pivotal role in determining the extent to which it influences hydrological processes and soil stability, contingent upon the biomass state of vegetation. Future research is imperative for advancing our comprehension of (i) the effects of the spatial distribution of vegetation and (ii) vegetation-climate feedback that induce alterations in atmospheric circulation.

CRediT authorship contribution statement

Guoding Chen: Writing – original draft, Software, Methodology, Conceptualization. **Ke Zhang:** Validation, Supervision, Methodology, Conceptualization, Funding acquisition. **Yunping Li:** Software, Methodology. **Jin Feng:** Visualization, Validation. **Thom Bogaard:** Writing – original draft, Supervision, Methodology, Conceptualization.

Declaration of competing interest

The authors declare that they have no known competing financial interests or personal relationships that could have appeared to influence the work reported in this paper.

Acknowledgements

This study was supported by National Key Research and Development Program of China (2023YFC3006505), Science and Technology Project of China Southern Power Grid Yunnan Power Grid Co., Ltd (YNKJXM20222329), Applied Scientific Research on the 'Three-Line Defense' Strengthening Foundation Project for Rainfall and Water Monitoring & Forecasting in Shandong Province (37000000025001720240235), Fundamental Research Funds for the Central Universities of China (B240203007), and the fund of National Key Laboratory of Water Disaster Prevention (524015222).

Appendix A. Supplementary data

Supplementary data to this article can be found online at https://doi.org/10.1016/j.jhydrol.2025.133225.

Data availability

Data will be made available on request.

References

Addo-Danso, S.D., Prescott, C.E., Smith, A.R., 2016. Methods for estimating root biomass and production in forest and woodland ecosystem carbon studies: a review. For. Ecol. Manage. 359, 332–351. https://doi.org/10.1016/j.foreco.2015.08.015.

Al-Omari, A.A., Shatnawi, N.N., Shbeeb, N.I., Istrati, D., Lagaros, N.D., Abdalla, K.M., 2024. Utilizing remote sensing and GIS techniques for flood hazard mapping and risk assessment. Civil Eng. J. 10, 1423–1436.

Alam, M., Jiang, Y.-J., Umar, M., Su, L.-J., Rahman, M., Ullah, F., 2021. Influence of drainage and root biomass on soil mechanical behavior in triaxial tests. Acta Geotech. 1–19.

Alemayehu, T., Van Griensven, A., Woldegiorgis, B.T., Bauwens, W., 2017. An improved SWAT vegetation growth module and its evaluation for four tropical ecosystems. Hydrol. Earth Syst. Sci. 21, 4449–4467.

Arnone, E., Caracciolo, D., Noto, L.V., Preti, F., Bras, R.L., 2016. Modeling the hydrological and mechanical effect of roots on shallow landslides. Water Resour. Res. 52, 8590–8612. https://doi.org/10.1002/2015WR018227.

Bai, P., Liu, X., Zhang, Y., Liu, C., 2018. Incorporating vegetation dynamics noticeably improved performance of hydrological model under vegetation greening. Sci. Total Environ. 643, 610–622. https://doi.org/10.1016/j.scitotenv.2018.06.233.

Bathurst, J.C., Fahey, B., Iroumé, A., Jones, J., 2020. Forests and floods: using field evidence to reconcile analysis methods. Hydrol. Process. 34, 3295–3310. https://doi.org/10.1002/hyp.13802.
Bayle, A., Carlson, B.Z., Zimmer, A., Vallée, S., Rabatel, A., Cremonese, E., Filippa, G., Dentant, C., Randin, C., Mainetti, A., 2023. Local environmental context drives heterogeneity of early succession dynamics in alpine glacier forefields. Biogeosciences 20, 1649–1669.
Bellot, J., Chirino, E., 2013. Hydrobal: an eco-hydrological modelling approach for assessing water balances in different vegetation types in semi-arid areas. Ecol. Model. 266, 30–41.
Bordoloi, S., Wang Wai Ng, C., 2020. The effects of vegetation traits and their stability functions in bio-engineered slopes: a perspective review. Eng. Geol., 105742 https://doi.org/10.1016/j.enggeo.2020.105742.
Bordoni, M., Cislaghi, A., Vercesi, A., Bischetti, G., Meisina, C., 2020. Effects of plant roots on soil shear strength and shallow landslide proneness in an area of northern Italian Apennines. Bull. Eng. Geol. Environ. 79, 3361–3381.
Bordoni, M., Vivaldi, V., Giarola, A., Valentino, R., Bittelli, M., Meisina, C., 2024. Comparison between mechanical and hydrological reinforcement effects of cultivated plants on shallow slope stability. Sci. Total Environ. 912, 168999.
Calder, I.R., Smyle, J., Aylward, B., 2007. Debate over flood-proofing effects of planting forests. Nature 450, 945.
Centre, D.H.P.C., 2022. DelftBlue Supercomputer (Phase 1).
Chen, G., Zhang, K., Wang, S., Xia, Y., Chao, L., 2023. iHydroSlide3D v1. 0: an advanced hydrological–geotechnical model for hydrological simulation and three-dimensional landslide prediction. Geosci. Model Dev. 16, 2915–2937. https://doi.org/10.5194/gmd-16-2915-2023.
Chen, H., Zhang, X., Abla, M., Lü, D., Yan, R., Ren, Q., Ren, Z., Yang, Y., Zhao, W., Lin, P., 2018. Effects of vegetation and rainfall types on surface runoff and soil erosion on steep slopes on the Loess Plateau, China. Catena 170, 141–149.
Chen, L., Huang, Z., Gong, J., Fu, B., Huang, Y., 2007. The effect of land cover/vegetation on soil water dynamic in the hilly area of the loess plateau, China. Catena 70, 200–208.
Chirico, G.B., Borga, M., Tarolli, P., Rigon, R., Preti, F., 2013. Role of vegetation on slope stability under transient unsaturated conditions. Proc. Environ. Sci. 19, 932–941.
Cislaghi, A., Chiaradia, E.A., Bischetti, G.B., 2017. Including root reinforcement variability in a probabilistic 3D stability model: root reinforcement variability in a probabilistic 3-D stability model. Earth Surf. Proc. Land. 42, 1789–1806. https://doi.org/10.1002/esp.4127.
Cislaghi, A., Rigon, E., Lenzi, M.A., Bischetti, G.B., 2018. A probabilistic multidimensional approach to quantify large wood recruitment from hillslopes in mountainous-forested catchments. Geomorphology 306, 108–127.
Cohen, D., Schwarz, M., Or, D., 2011. An analytical fiber bundle model for pullout mechanics of root bundles. J. Geophys. Res. 116, F03010. https://doi.org/10.1029/2010JF001886.
Coppin, N.J., Richards, I.G., 1990. Use of Vegetation in Civil Engineering. Ciria Butterworths.
Coyle, D.R., Coleman, M.D., Aubrey, D.P., 2008. Above- and below-ground biomass accumulation, production, and distribution of sweetgum and loblolly pine grown with irrigation and fertilization. Can. J. For. Res. 38, 1335–1348. https://doi.org/10.1139/X07-231.
De Moraes, M.T., Bengough, A.G., Debiasi, H., Franchini, J.C., Levien, R., Schnepf, A., Leitner, D., 2018. Mechanistic framework to link root growth models with weather and soil physical properties, including example applications to soybean growth in Brazil. Plant Soil 428, 67–92.
Donohue, R.J., Roderick, M.L., McVicar, T.R., 2010. Can dynamic vegetation information improve the accuracy of Budyko's hydrological model? J. Hydrol. 390, 23–34.
Du, H., Liu, L., Su, L., Zeng, F., Wang, K., Peng, W., Zhang, H., Song, T., 2019. Seasonal changes and vertical distribution of fine root biomass during vegetation restoration in a karst area, Southwest China. Front. Plant Sci. 9, 2001.
Ekanayake, J.C., Phillips, C.J., 1999. A method for stability analysis of vegetated hillslopes: an energy approach. Can. Geotech. J. 36, 1172–1184.
El Kateb, H., Zhang, H., Zhang, P., Mosandl, R., 2013. Soil erosion and surface runoff on different vegetation covers and slope gradients: a field experiment in Southern Shaanxi Province, China. Catena 105, 1–10.
Evette, A., Labonne, S., Rey, F., Liebault, F., Jancke, O., Girel, J., 2009. History of bioengineering techniques for erosion control in rivers in Western Europe. Environ. Manag. 43, 972–984.
Fatichi, S., Ivanov, V.Y., Caporali, E., 2011. Simulation of future climate scenarios with a weather generator. Adv. Water Resour. 34, 448–467. https://doi.org/10.1016/j.advwatres.2010.12.013.
Feng, S., Liu, H.W., Ng, C.W.W., 2020. Analytical analysis of the mechanical and hydrological effects of vegetation on shallow slope stability. Comput. Geotech. 118, 103335. https://doi.org/10.1016/j.compgeo.2019.103335.
Flamig, Z.L., Vergara, H., Gourley, J.J., 2020. The ensemble framework for flash flood forecasting (EF5) v1.2: description and case study. Geosci. Model Dev. 13, 4943–4958. https://doi.org/10.5194/gmd-13-4943-2020.
García-Gamero, V., Peña, A., Laguna, A., Giráldez, J.V., Vanwalleghem, T., 2021. Factors controlling the asymmetry of soil moisture and vegetation dynamics in a hilly Mediterranean catchment. J. Hydrol. 598, 126207.
Gilmour, D.A., 1968. Hydrological investigations of soil and vegetation types in the lower Cotter catchment. Aust. For. 32, 243–256.
Green, K.C., Alila, Y., 2012. A paradigm shift in understanding and quantifying the effects of forest harvesting on floods in snow environments. Water Resour. Res. 48, 2012WR012449. https://doi.org/10.1029/2012WR012449.
Hales, T.C., Miniat, C.F., 2017. Soil moisture causes dynamic adjustments to root reinforcement that reduce slope stability. Earth Surf. Proc. Land. 42, 803–813.
Han, B., Jin, X., Xiang, X., Rui, S., Zhang, X., Jin, Z., Zhou, Y., 2021. An integrated evaluation framework for Land-Space ecological restoration planning strategy making in rapidly developing area. Ecol. Ind. 124, 107374.
Hartmann, A., Šimůnek, J., Aidoo, M.K., Seidel, S.J., Lazarovitch, N., 2018. Implementation and application of a root growth module in HYDRUS. Vadose Zone J. 17, 170040. https://doi.org/10.2136/vzj2017.02.0040.
Hong, Y., Adler, R., Huffman, G., 2006. Evaluation of the potential of NASA multi-satellite precipitation analysis in global landslide hazard assessment. Geophys. Res. Lett. 33. https://doi.org/10.1029/2006GL028010.
Huo, H., Sun, C., 2021. Spatiotemporal variation and influencing factors of vegetation dynamics based on Geodetector: a case study of the northwestern Yunnan Plateau, China. Ecol. Indic. 130, 108005.
Jin, X.-Y., Jin, H.-J., Iwahana, G., Marchenko, S.S., Luo, D.-L., Li, X.-Y., Liang, S.-H., 2021. Impacts of climate-induced permafrost degradation on vegetation: a review. Adv. Clim. Chang. Res. 12, 29–47.
Jolly, W.M., Nemani, R., Running, S.W., 2005. A generalized, bioclimatic index to predict foliar phenology in response to climate. Glob. Chang. Biol. 11, 619–632. https://doi.org/10.1111/j.1365-2486.2005.00930.x.
Katul, G.G., Oren, R., Manzoni, S., Higgins, C., Parlange, M.B., 2012. Evapotranspiration: a process driving mass transport and energy exchange in the soil-plant-atmosphere-climate system. Rev. Geophys. 50.
Kim, D., Im, S., Lee, C., Woo, C., 2013. Modeling the contribution of trees to shallow landslide development in a steep, forested watershed. Ecol. Eng. 61, 658–668.
Kumar, P., Debele, S.E., Sahani, J., Rawat, N., Marti-Cardona, B., Alfieri, S.M., Basu, B., Basu, A.S., Bowyer, P., Charizopoulos, N., Gallotti, G., Jaakko, J., Leo, L.S., Loupis, M., Menenti, M., Mickovski, S.B., Mun, S.-J., Gonzalez-Ollauri, A., Pfeiffer, J., Pilla, F., Pröll, J., Rutzinger, M., Santo, M.A., Sannigrahi, S., Spyrou, C., Tuomenvirta, H., Zieher, T., 2021. Nature-based solutions efficiency evaluation against natural hazards: modelling methods, advantages and limitations. Sci. Total Environ., 147058 https://doi.org/10.1016/j.scitotenv.2021.147058.
Kuraś, P.K., Alila, Y., Weiler, M., 2012. Forest harvesting effects on the magnitude and frequency of peak flows can increase with return period: forest harvesting impacts on peak flows. Water Resour. Res. 48. https://doi.org/10.1029/2011WR010705.
Lai, J., Yang, B., Lin, D., Kerkhoff, A.J., Ma, K., 2013. The allometry of coarse root biomass: log-transformed linear regression or nonlinear regression? PLoS One 8, e77007.
Lann, T., Bao, H., Lan, H., Zheng, H., Yan, C., 2024. Hydro-mechanical effects of vegetation on slope stability: a review. Sci. Total Environ., 171691
Leitner, D., Klepsch, S., Bodner, G., Schnepf, A., 2010. A dynamic root system growth model based on L-systems: tropisms and coupling to nutrient uptake from soil. Plant Soil 332, 177–192. https://doi.org/10.1007/s11104-010-0284-7.
Lenhart, T., Eckhardt, K., Fohrer, N., Frede, H.-G., 2002. Comparison of two different approaches of sensitivity analysis. Phys. Chem. Earth Parts a/b/c 27, 645–654.
Li, J., 2007. Flora of China. Harv. Pap. Bot. 13, 301–302.
Li, Y., Piao, S., Li, L.Z.X., Chen, A., Wang, X., Ciais, P., Huang, L., Lian, X., Peng, S., Zeng, Z., 2018. Divergent hydrological response to large-scale afforestation and vegetation greening in China. Sci. Adv. 4, eaar4182.
Li, Z., Chen, M., Gao, S., Luo, X., Gourley, J.J., Kirstetter, P., Yang, T., Kolar, R., McGovern, A., Wen, Y., Rao, B., Yami, T., Hong, Y., 2021. CREST-iMAP v1.0: a fully coupled hydrologic-hydraulic modeling framework dedicated to flood inundation mapping and prediction. Environ. Model. Softw. 141, 105051. https://doi.org/10.1016/j.envsoft.2021.105051.
Lin, S., Shaw, D., Ho, M.-C., 2008. Why are flood and landslide victims less willing to take mitigation measures than the public? Nat. Hazards 44, 305–314.
Liu, H.W., Feng, S., Ng, C.W.W., 2016. Analytical analysis of hydraulic effect of vegetation on shallow slope stability with different root architectures. Comput. Geotech. 80, 115–120. https://doi.org/10.1016/j.compgeo.2016.06.006.
Lu, N., Godt, J.W., 2013. Hillslope Hydrology and Stability. Cambridge University Press.
Luan, J., Miao, P., Tian, X., Li, X., Ma, N., Faiz, M.A., Xu, Z., Zhang, Y., 2022. Estimating hydrological consequences of vegetation greening. J. Hydrol. 611, 128018.
Luo, Y., Yang, Y., Yang, D., Zhang, S., 2020a. Quantifying the impact of vegetation changes on global terrestrial runoff using the Budyko framework. J. Hydrol. 590, 125389.
Luo, Y., Zhang, X., Liu, X., Ficklin, D., Zhang, M., 2008. Dynamic modeling of organophosphate pesticide load in surface water in the northern San Joaquin Valley watershed of California. Environ. Pollut. 156, 1171–1181.
Luo, Y., Wang, X., Ouyang, Z., Lu, F., Feng, L., Tao, J., 2020b. A review of biomass equations for China's tree species. Earth Syst. Sci. Data 12, 21–40. https://doi.org/10.5194/essd-12-21-2020.
Ma, L., Hurtt, G., Ott, L., Sahajpal, R., Fisk, J., Lamb, R., Tang, H., Flanagan, S., Chini, L., Chatterjee, A., Sullivan, J., 2022. Global evaluation of the ecosystem demography model (ED v3.0). Geosci. Model Dev. 15, 1971–1994. https://doi.org/10.5194/gmd-15-1971-2022.
Meinen, C., Hertel, D., Leuschner, C., 2009. Root growth and recovery in temperate broad-leaved forest stands differing in tree species diversity. Ecosystems 12, 1103–1116.
Mergili, M., Marchesini, I., Alvioli, M., Metz, M., Schneider-Muntau, B., Rossi, M., Guzzetti, F., 2014. A Strategy for GIS-based 3-D slope stability modelling over large areas. Geosci. Model Dev. 7, 2969–2982. https://doi.org/10.5194/gmd-7-2969-2014.
Mu, Q., Zhao, M., Running, S.W., 2011. Improvements to a MODIS global terrestrial evapotranspiration algorithm. Remote Sens. Environ. 115, 1781–1800. https://doi.org/10.1016/j.rse.2011.02.019.
Ng, C.W.W., Liu, H.W., Feng, S., 2015. Analytical solutions for calculating pore-water pressure in an infinite unsaturated slope with different root architectures. Can. Geotech. J. 52, 1981–1992. https://doi.org/10.1139/cgj-2015-0001.

Nwobi, C.J., Williams, M., 2021. Natural and anthropogenic variation of stand structure and aboveground biomass in Niger Delta Mangrove forests. Front. For. Global Change 4, 746671. https://doi.org/10.3389/ffgc.2021.746671.
Parr, D., Wang, G., Bjerklie, D., 2015. Integrating remote sensing data on evapotranspiration and leaf area index with hydrological modeling: impacts on model performance and future predictions. J. Hydrometeorol. 16, 2086–2100. https://doi.org/10.1175/JHM-D-15-0009.1.
Pollen, N., 2007. Temporal and spatial variability in root reinforcement of streambanks: accounting for soil shear strength and moisture. Catena 69, 197–205.
Pollen, N., Simon, A., 2005. Estimating the mechanical effects of riparian vegetation on stream bank stability using a fiber bundle model: modeling root reinforcement of stream banks. Water Resour. Res. 41. https://doi.org/10.1029/2004WR003801.
Preti, F., Dani, A., Noto, L.V., Arnone, E., 2022. On the Leonardo's rule for the assessment of root profile. Ecol. Eng. 179, 106620. https://doi.org/10.1016/j.ecoleng.2022.106620.
Rattanarat, J., Jaroensutasinee, K., Jaroensutasinee, M., Sparrow, E.B., 2024. Government policy influence on land use and land cover changes: a 30-year analysis. Emerg. Sci. J. 8, 1783–1797.
Savoy, P., Mackay, D.S., 2015. Modeling the seasonal dynamics of leaf area index based on environmental constraints to canopy development. Agric. For. Meteorol. 200, 46–56. https://doi.org/10.1016/j.agrformet.2014.09.019.
Schmaltz, E.M., Mergili, M., 2018. Integration of root systems into a GIS-based slip surface model: computational experiments in a generic hillslope environment. Landslides 15, 1561–1575. https://doi.org/10.1007/s10346-018-0970-8.
Schmidt, K., Roering, J., Stock, J., Dietrich, W., Montgomery, D., Schaub, T., 2001. The variability of root cohesion as an influence on shallow landslide susceptibility in the Oregon Coast Range. Can. Geotech. J. 38, 995–1024.
Schwarz, M., Cohen, D., Or, D., 2012. Spatial characterization of root reinforcement at stand scale: theory and case study. Geomorphology 171–172, 190–200. https://doi.org/10.1016/j.geomorph.2012.05.020.
Schwarz, M., Giadrossich, F., Cohen, D., 2013. Modeling root reinforcement using a root-failure Weibull survival function. Hydrol. Earth Syst. Sci. 17, 4367–4377. https://doi.org/10.5194/hess-17-4367-2013.
Schwarz, M., Lehmann, P., Or, D., 2010a. Quantifying lateral root reinforcement in steep slopes \textendash from a bundle of roots to tree stands. Earth Surf. Proc. Land. 35, 354–367. https://doi.org/10.1002/esp.1927.
Schwarz, M., Preti, F., Giadrossich, F., Lehmann, P., Or, D., 2010b. Quantifying the Role of Vegetation in Slope Stability: A Case Study in Tuscany (Italy). Ecol. Eng. 36, 285–291. https://doi.org/10.1016/j.ecoleng.2009.06.014.
Setiawan, B.I., 2020. A simple method to determine patterns of wet and dry seasons. IOP Conf. Ser.: Earth Environ. Sci.
Sheng, F., Liu, S., Zhang, T., Liu, G., Liu, Z., 2022. Quantitative assessment of the impact of precipitation and vegetation variation on flooding under discrete and continuous rainstorm conditions. Ecol. Ind. 144, 109477.
Sloan, V.L., Fletcher, B.J., Press, M.C., Williams, M., Phoenix, G.K., 2013. Leaf and fine root carbon stocks and turnover are coupled across Arctic ecosystems. Glob. Chang. Biol. 19, 3668–3676.
Stephens, C.M., Lall, U., Johnson, F., Marshall, L.A., 2021. Landscape changes and their hydrologic effects: Interactions and feedbacks across scales. Earth-Sci. Rev. 212, 103466.
Stöckli, R., Rutishauser, T., Dragoni, D., O'Keefe, J., Thornton, P.E., Jolly, M., Lu, L., Denning, A.S., 2008. Remote sensing data assimilation for a prognostic phenology model: data assimilation and phenology modeling. J. Geophys. Res. Biogeo. 113. https://doi.org/10.1029/2008JG000781.
Stokes, A., Douglas, G.B., Fourcaud, T., Giadrossich, F., Gillies, C., Hubble, T., Kim, J.H., Loades, K.W., Mao, Z., McIvor, I.R., 2014. Ecological mitigation of hillslope instability: ten key issues facing researchers and practitioners. Plant Soil 377, 1–23.
Sulla-Menashe, D., Friedl, M.A., 2018. User guide to collection 6 MODIS land cover (MCD12Q1 and MCD12C1) product, USGS: Reston, VA, USA, 1, 18.
Tesemma, Z., Wei, Y., Peel, M., Western, A., 2015. Including the dynamic relationship between climatic variables and leaf area index in a hydrological model to improve streamflow prediction under a changing climate. Hydrol. Earth Syst. Sci. 19, 2821–2836.
Tran, T.V., Alvioli, M., Lee, G., An, H.U., 2018. Three-dimensional, time-dependent modeling of rainfall-induced landslides over a digital landscape: a case study. Landslides 15, 1071–1084. https://doi.org/10.1007/s10346-017-0931-7.
Tron, S., Bodner, G., Laio, F., Ridolfi, L., Leitner, D., 2015. Can diversity in root architecture explain plant water use efficiency? A modeling study. Ecol. Model. 312, 200–210. https://doi.org/10.1016/j.ecolmodel.2015.05.028.
Tron, S., Dani, A., Laio, F., Preti, F., Ridolfi, L., 2014. Mean root depth estimation at landslide slopes. Ecol. Eng. 69, 118–125. https://doi.org/10.1016/j.ecoleng.2014.03.019.
Vuuren, D.P., Edmonds, J., Kainuma, M., Riahi, K., Thomson, A., Hibbard, K., Hurtt, G.C., Kram, T., Krey, V., Lamarque, J.-F., 2011. The representative concentration pathways: an overview. Clim. Change 109, 5–31.
Vergani, C., Giadrossich, F., Buckley, P., Conedera, M., Pividori, M., Salbitano, F., Rauch, H., Lovreglio, R., Schwarz, M., 2017. Root reinforcement dynamics of European coppice woodlands and their effect on shallow landslides: a review. Earth Sci. Rev. 167, 88–102.
Waldron, L., 1977. The shear resistance of root-permeated homogeneous and stratified soil. Soil Sci. Soc. Am. J. 41, 843–849.
Waldron, L., Dakessian, S., 1981. Soil reinforcement by roots: calculation of increased soil shear resistance from root properties. Soil Sci. 132, 427–435.
Wang, J., Hong, Y., Li, L., Gourley, J.J., Khan, S.I., Yilmaz, K.K., Adler, R.F., Policelli, F. S., Habib, S., Irwn, D., Limaye, A.S., Korme, T., Okello, L., 2011. The coupled routing and excess storage (CREST) distributed hydrological model. Hydrol. Sci. J. 56, 84–98. https://doi.org/10.1080/02626667.2010.543087.
Wang, S., Zhang, K., van Beek, L.P.H., Tian, X., Bogaard, T.A., 2020. Physically-based landslide prediction over a large region: scaling low-resolution hydrological model results for high-resolution slope stability assessment. Environ. Model. Softw. 124, 104607. https://doi.org/10.1016/j.envsoft.2019.104607.
Wasko, C., Nathan, R., Stein, L., O'Shea, D., 2021. Evidence of shorter more extreme rainfalls and increased flood variability under climate change. J. Hydrol. 603, 126994.
Wieder, W.R., Boehnert, J., Bonan, G.B., Langseth, M., 2014. Regridded harmonized world soil database v1. 2. ORNL DAAC.
Wu, T.H., McKinnell III, W.P., Swanston, D.N., 1979. Strength of tree roots and landslides on Prince of Wales Island, Alaska. Can. Geotech. J. 16, 19–33.
Xu, X., Medvigy, D., Powers, J.S., Becknell, J.M., Guan, K., 2016. Diversity in plant hydraulic traits explains seasonal and inter-annual variations of vegetation dynamics in seasonally dry tropical forests. New Phytol. 212, 80–95. https://doi.org/10.1111/nph.14009.
Yanfatriani, E., Marzuki, M., Vonnisa, M., Razi, P., Hapsoro, C.A., Ramadhan, R., Yusnaini, H., 2024. Extreme rainfall trends and hydrometeorological disasters in tropical regions: implications for climate resilience. Emerg. Sci. J. 8, 1860–1874.
Yu, Y., Wei, W., Chen, L., Feng, T., Daryanto, S., 2019. Quantifying the effects of precipitation, vegetation, and land preparation techniques on runoff and soil erosion in a Loess Watershed of China. Sci. Total Environ. 652, 755–764. https://doi.org/10.1016/j.scitotenv.2018.10.255.
Zhang, B., Tian, L., Yang, Y., He, X., 2022a. Revegetation does not decrease water yield in the Loess Plateau of China. Geophys. Res. Lett. https://doi.org/10.1029/2022GL098025.
Zhang, B., Tian, L., Zhao, X., Wu, P., 2021. Feedbacks between vegetation restoration and local precipitation over the Loess Plateau in China. Sci. China Earth Sci. 64, 920–931.
Zhang, K., Chen, G., Xia, Y., Wang, S., 2022b. An ensemble-based, remote-sensing-driven, flood-landslide early warning system. Remote Sens. Water-Related Hazards 123–134.
Zhang, K., Xue, X., Hong, Y., Gourley, J.J., Lu, N., Wan, Z., Hong, Z., Wooten, R., 2016. iCRESTRIGRS: a coupled modeling system for cascading flood-landslide disaster forecasting. Hydrol. Earth Syst. Sci. 20, 5035–5048. https://doi.org/10.5194/hess-20-5035-2016.
Zhang, K., Ali, A., Antonarakis, A., Moghaddam, M., Saatchi, S., Tabatabaeenejad, A., Chen, R., Jaruwatanadilok, S., Cuenca, R., Crow, W.T., 2019a. The sensitivity of North American terrestrial carbon fluxes to spatial and temporal variation in soil moisture: an analysis using radar-derived estimates of root-zone soil moisture. J. Geophys. Res.: Biogeosci. 124, 3208–3231.
Zhang, S., Li, Z., Hou, X., Yi, Y., 2019b. Impacts on watershed-scale runoff and sediment yield resulting from synergetic changes in climate and vegetation. Catena 179, 129–138. https://doi.org/10.1016/j.catena.2019.04.007.
Zhang, X., Yu, G.Q., Li, Z.B., Li, P., 2014. Experimental study on slope runoff, erosion and sediment under different vegetation types. Water Resour. Manag. 28, 2415–2433. https://doi.org/10.1007/s11269-014-0603-5.
Zhao, C., Gao, J.e., Huang, Y., Wang, G., Zhang, M., 2016. Effects of vegetation stems on hydraulics of overland flow under varying water discharges. Land Degrad. Dev. 27, 748–757. https://doi.org/10.1002/ldr.2423.